Spectroscopy of Transition Region and Corona

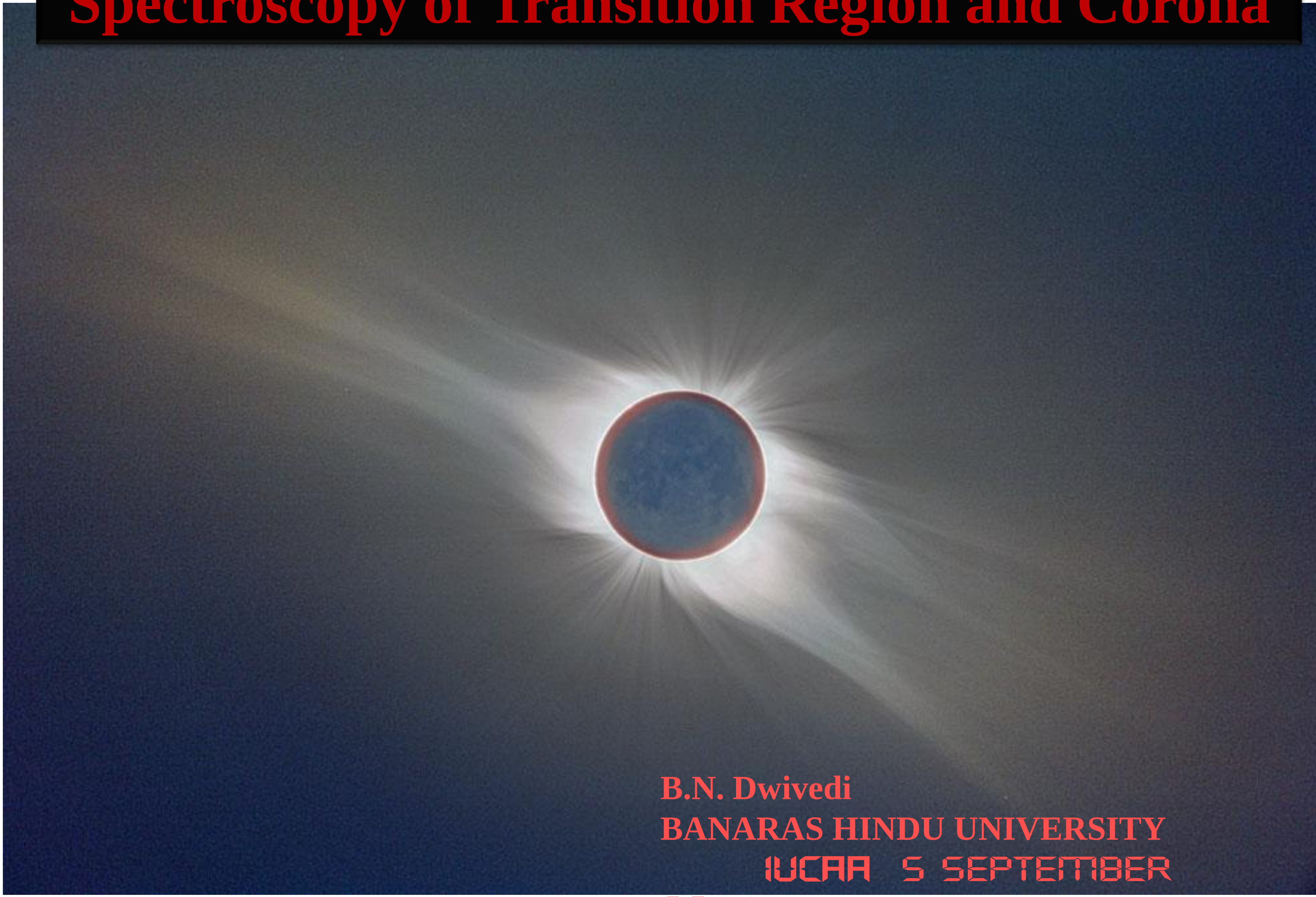

B.N. Dwivedi
BANARAS HINDU UNIVERSITY
IUCAA 5 September 2011

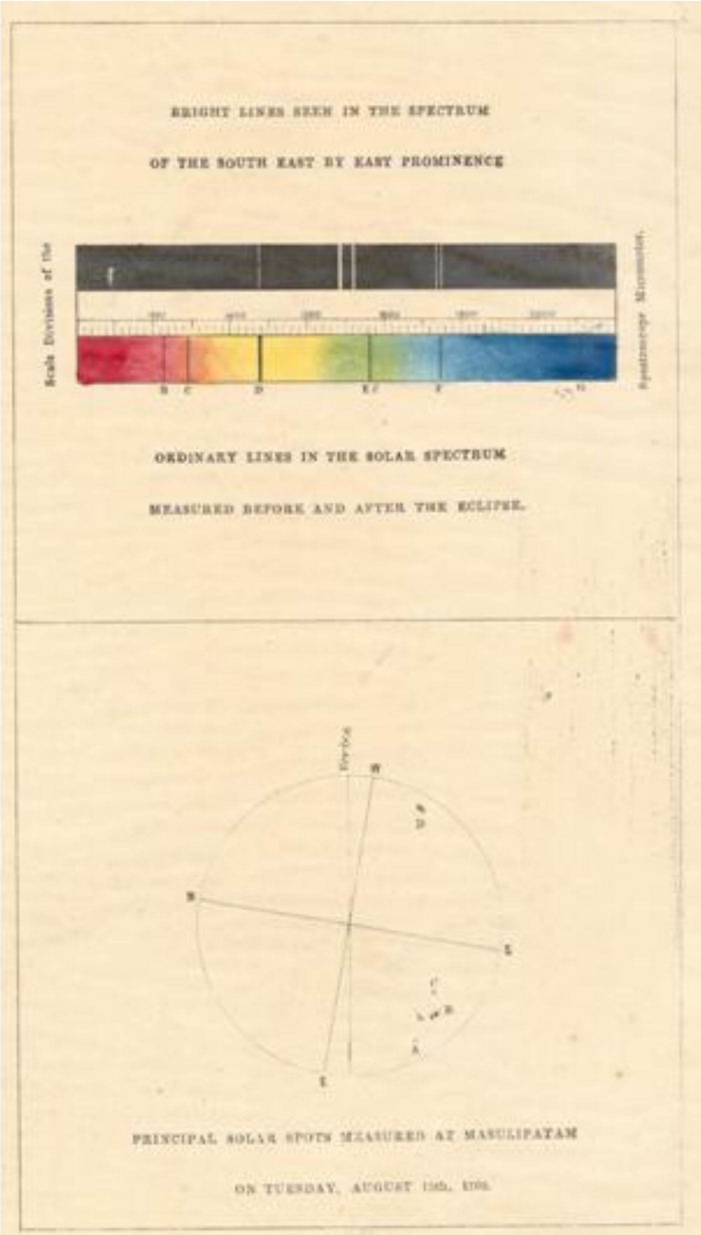

Discovery of Helium →
TSE 18 August 1868, Guntur, India.

Einstein's theory of relativity →
TSE 1919 →
Bending of light in the Sun's vicinity.

Hand-coloured sketch of the solar spectrum during TSE on 18 August 1868.
(Credit: IIA, Bangalore)

C.A. Young & W. Harkness → Solar TSE 1869:
530 nm 'Green' line

E.O.Hulburt (1938)

"ultraviolet light, X-rays or particles of zero average charge" → Responsible for the E-layer of the Earth's ionosphere.

Hannes Alfvén (1941)

"It is pointed out that several facts indicate the existence in the solar corona of particles (electrons and ions) having energies far above thermal energies.

It is tentatively suggested that the corona might consist altogether of such high energy particles which is the same as to say that it is heated to an extremely high temperature."

Bengt Edlén (1943)

Green coronal line (530.3 nm) from Fe^{+13}.

Green (530.3 nm) & Red (637.5 nm) coronal lines → Forbidden lines in the spectra of Fe XIV (Fe^{+13}) & Fe X (Fe^{+9})

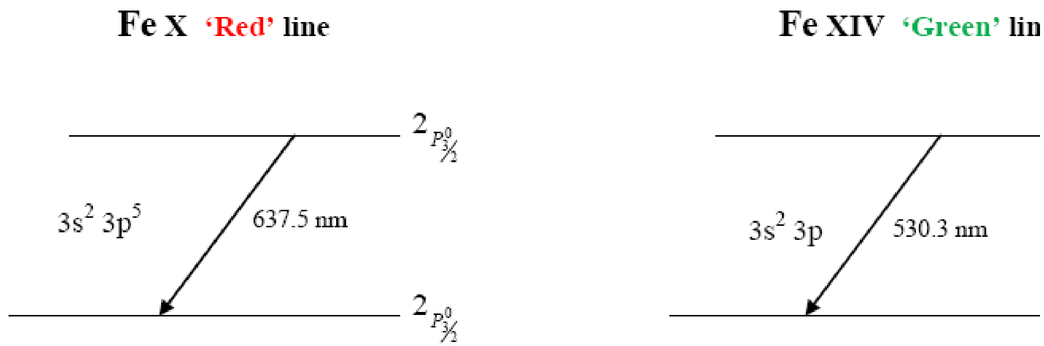

'Red' and 'Green' coronal lines.

These pioneering investigations → Basic properties of the corona → (i) Rarefied Gas & (ii) Very High Temperature.

Soft X-ray and ultraviolet emission (from 0.2 to 300 nm) in the post-World War II → Existence of the Corona's High Temperature.

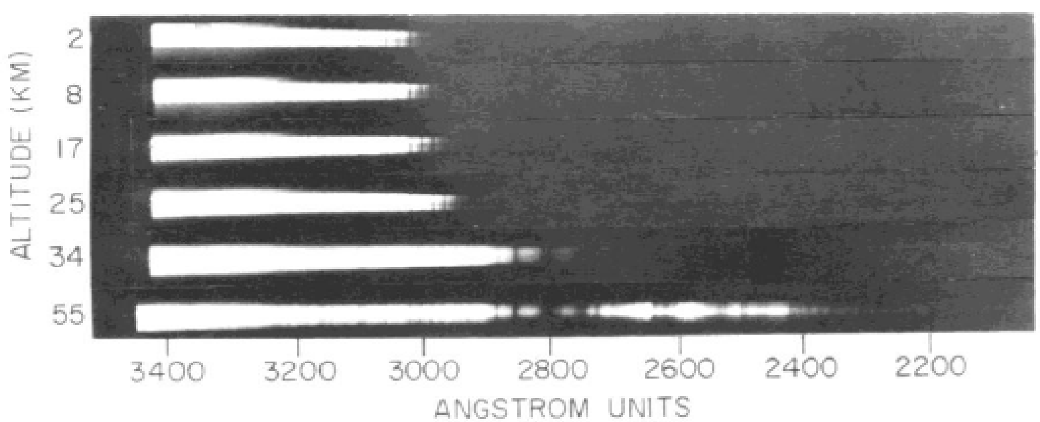

The first photograph of the solar ultraviolet spectrum, obtained with an instrument built by the US Naval Research Laboratory on a (captured German military V2) rocket launched in October 1946.

Radiation Mechanisms

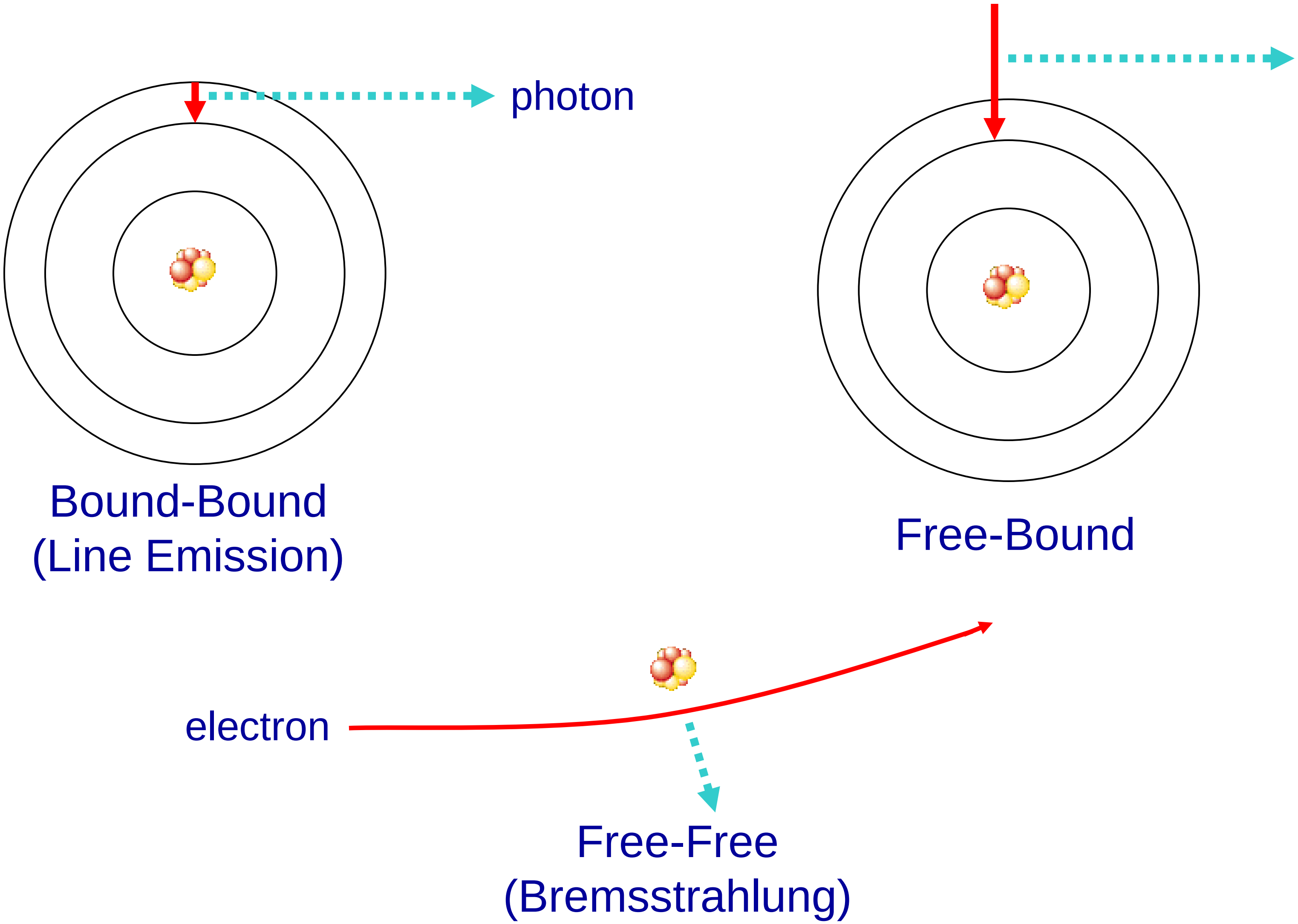

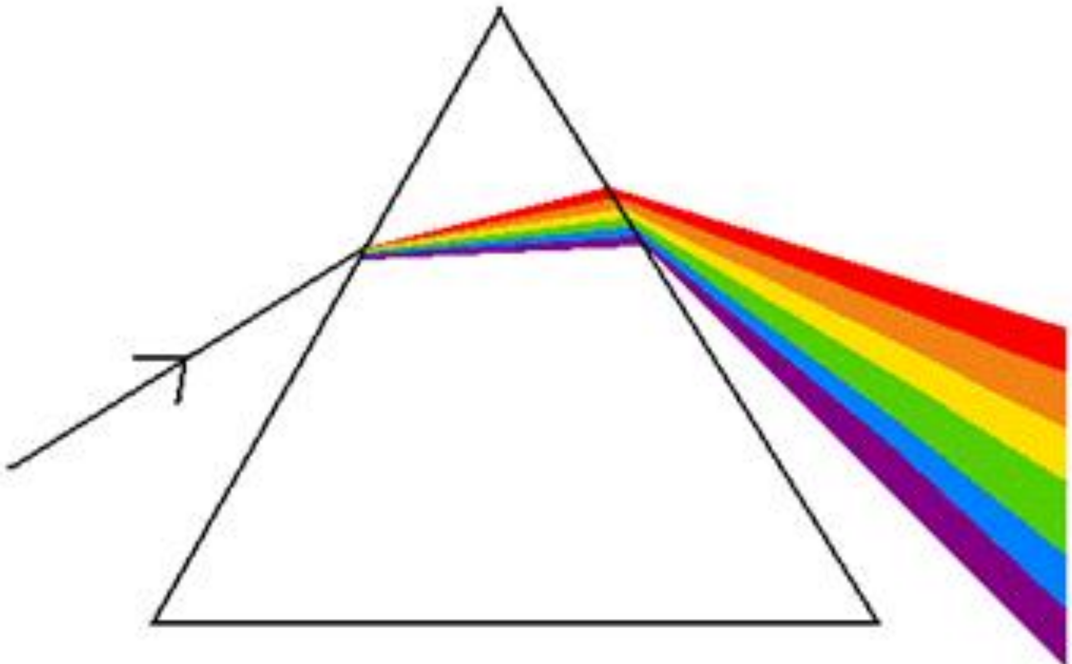

Dispersion of a multi-wavelength light source ⟶ a spectrum

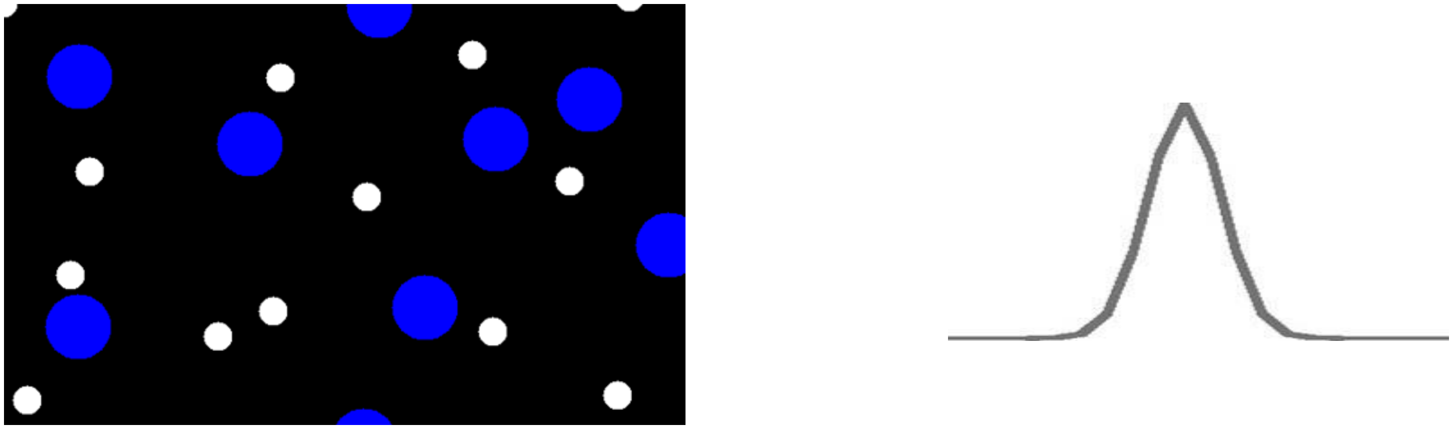

Less Particle Density ⇒ Lower Intensity (Fainter Line)

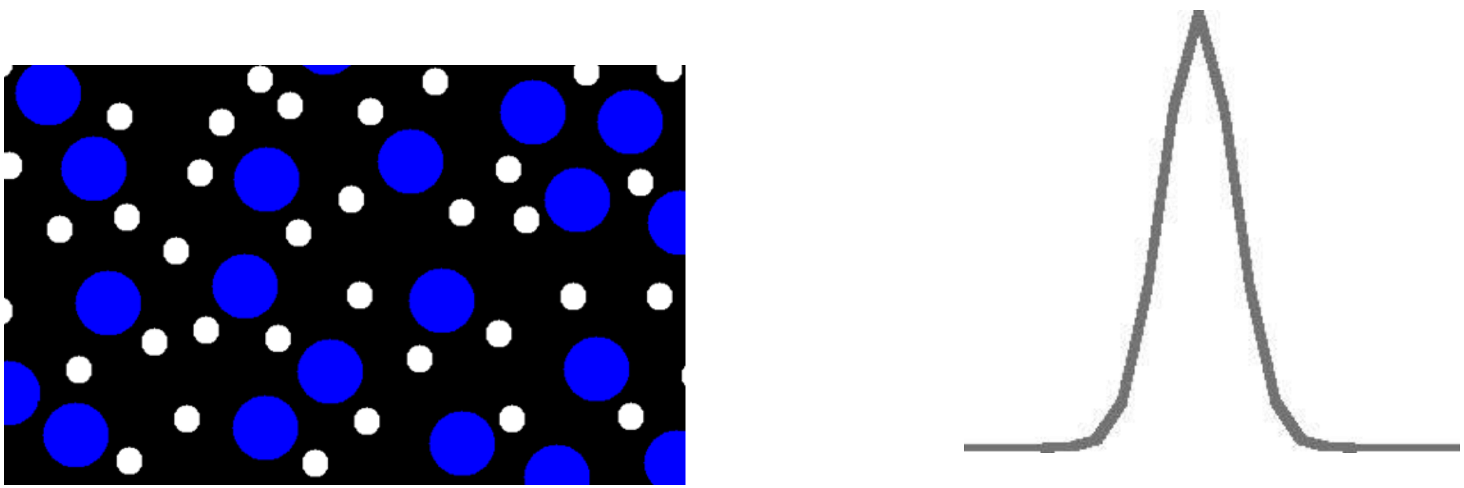

More Particle Density ⇒ Higher Intensity (Brighter Line)

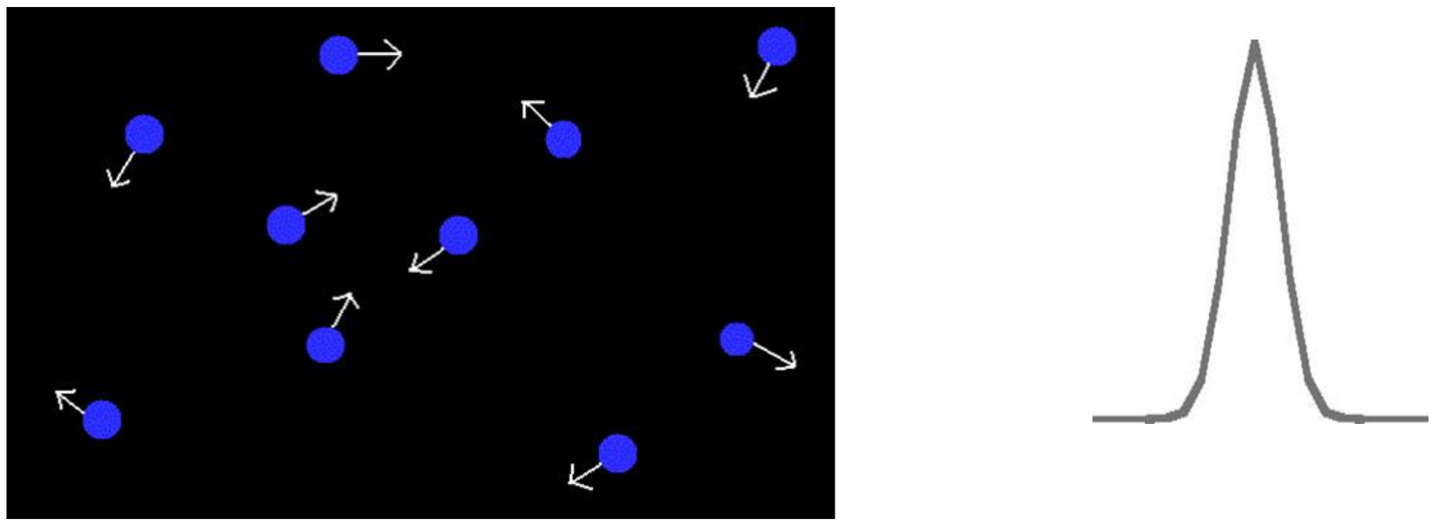

Slower Random Motion ⇒ Narrower Width

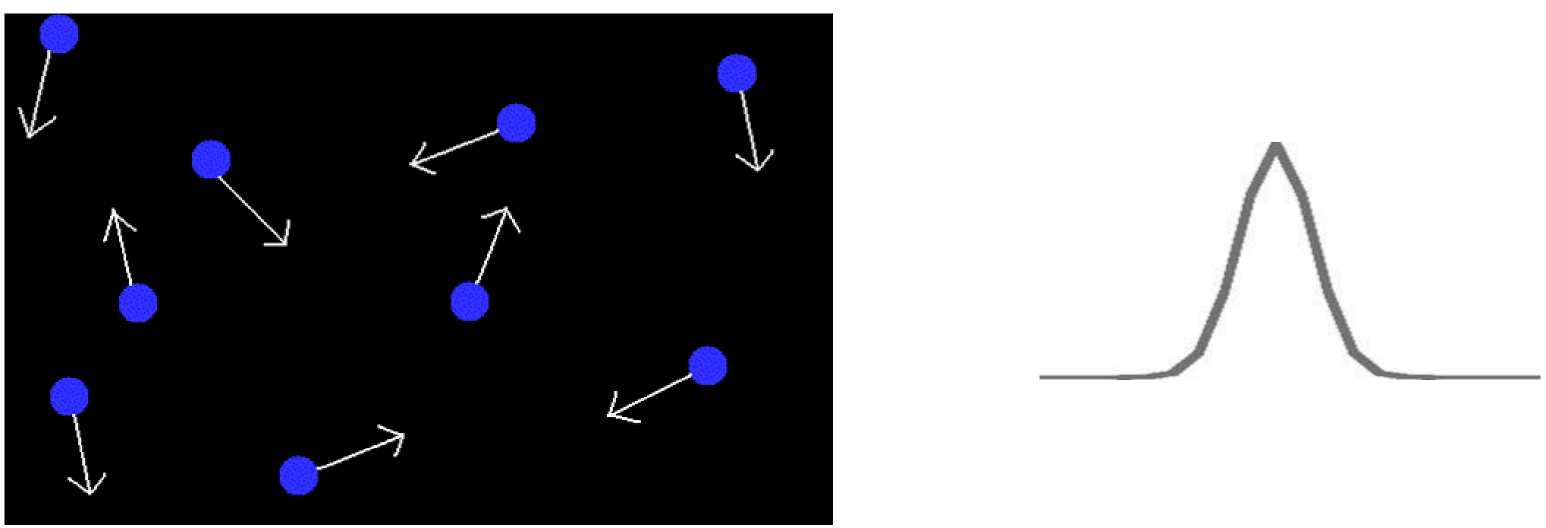

Faster Random Motion ⇒ Wider Width

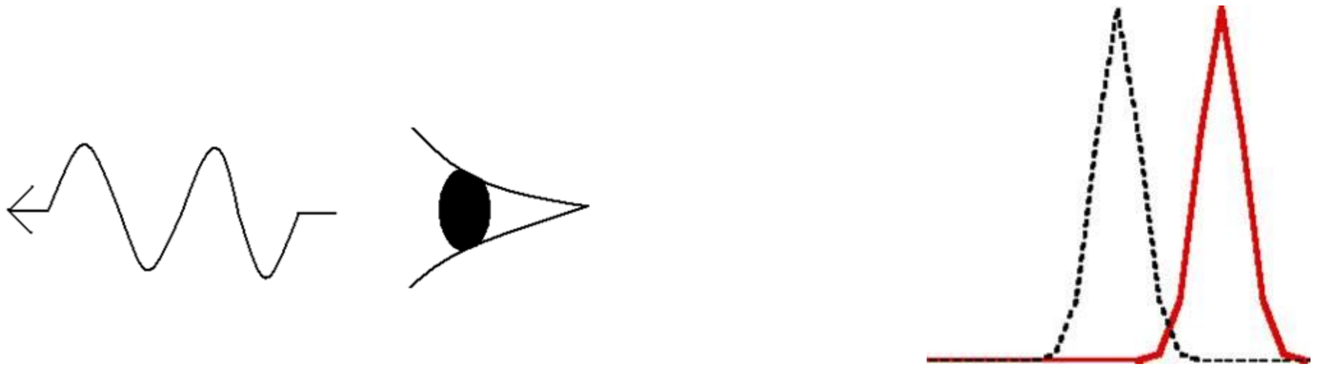

Source Moving Away from us ⇒ Red Shift (Longer Wavelength)

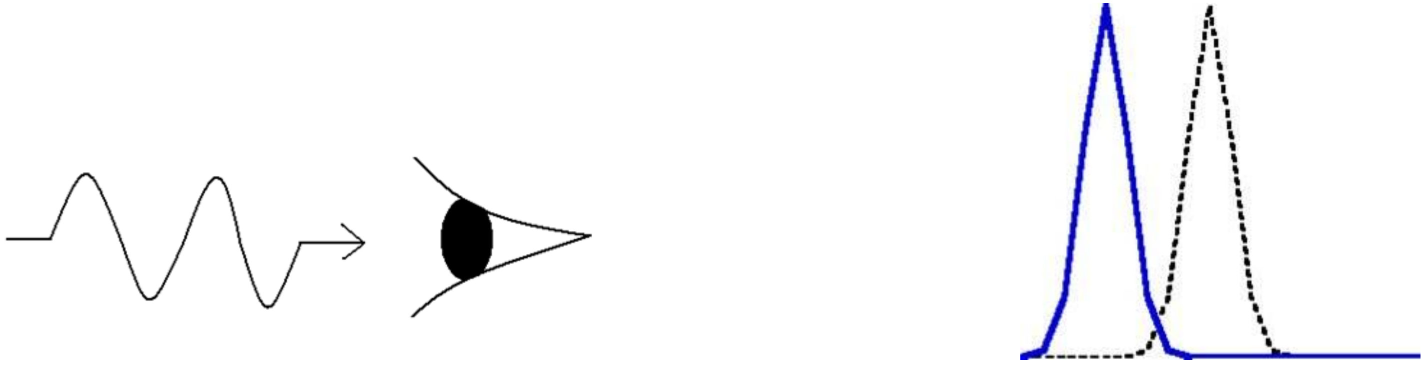

Source Moving toward us ⇒ Blue Shift (Shorter Wavelength)

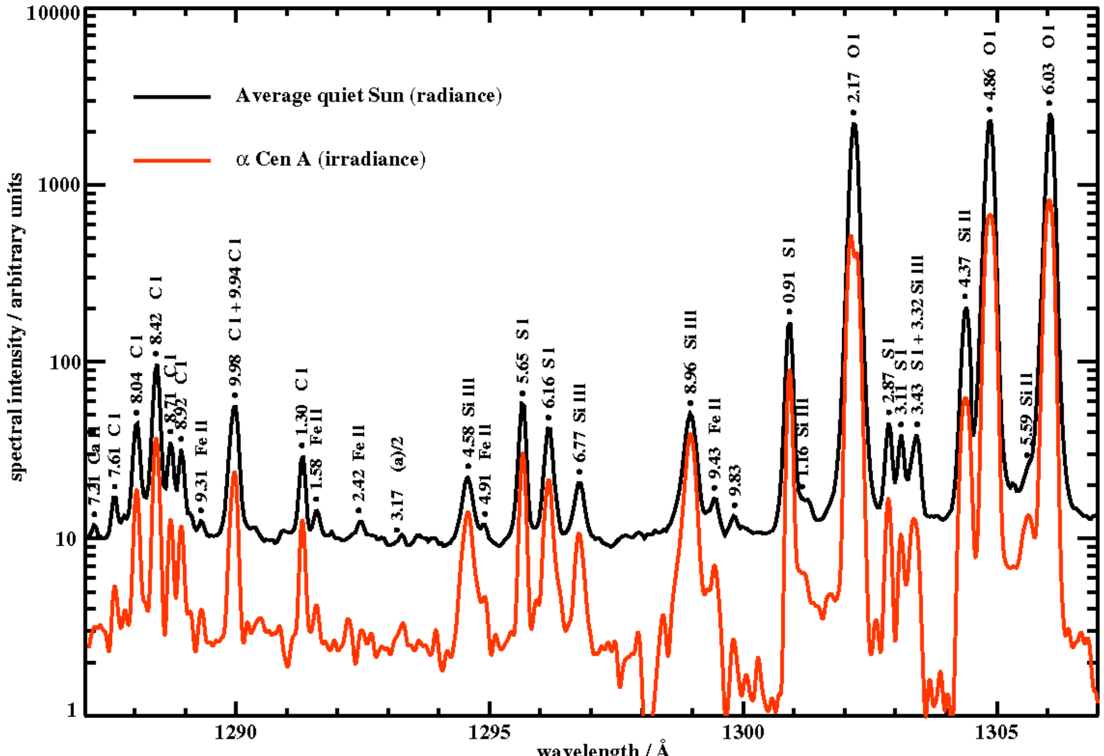

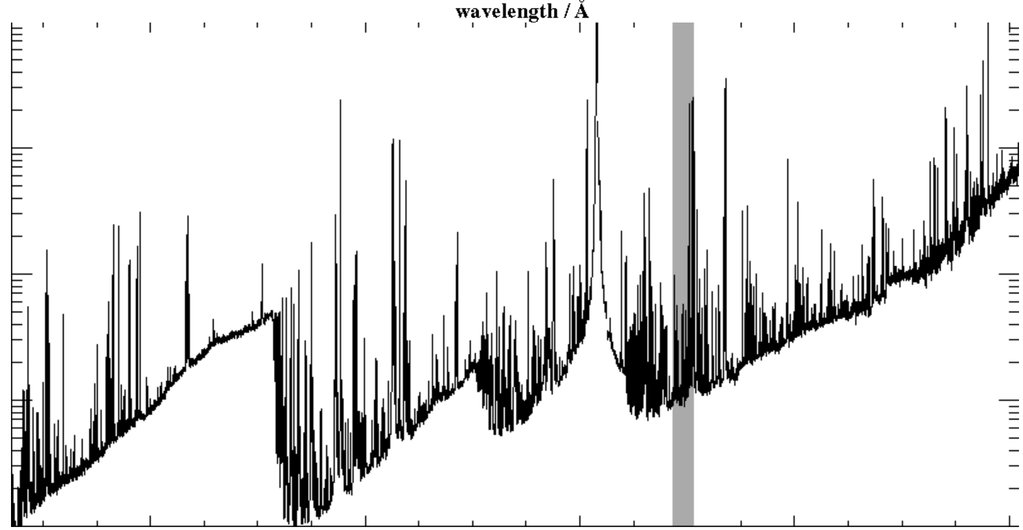

SUMER spectral atlas is the best-ever analysis of the Sun's ultraviolet light, from 670 Å to 1609 Å & identifies some 1100 distinct emission lines, of which more than 150 had not been recorded or identified before *SOHO*. (Curdt *et al.* 2001)

Outstanding Questions

Dynamical cause of the photospheric and chromospheric brightenings in the presence of magnetic field

FIP Effect (Abundance Anomalies)

Various magnetic configurations – Flares of different kinds

Dynamics of interplanetary holocaust $\Rightarrow$ CMEs & Flares

- Terrestrial Magnetosphere
- Geomagnetic Storm
- Cosmic Ray Modulation in the Heliosphere
- Shape of Heliopause

Million Degree Hot Corona

Solar Wind

- Why a star is compelled to produce a supersonic wind?
- Why the gas in coronal hole has a temperature $\geq 10^6$ K?

Observational Testing

Physical Parameters: N_e, T_e, flow speeds, ⟶

Not directly measurable:

- **Magnetic field strength**
- **Resistivity**
- **Viscosity**
- **Turbulence**
- **Waves, ---**

Powerful New Tools:

- **Detection of MHD waves by TRACE & EIT.**
- **Spectroscopic measurements of line-widths by SUMER & CDS.**
- **Ion & electron temperature anisotropy measurements with UVCS.**

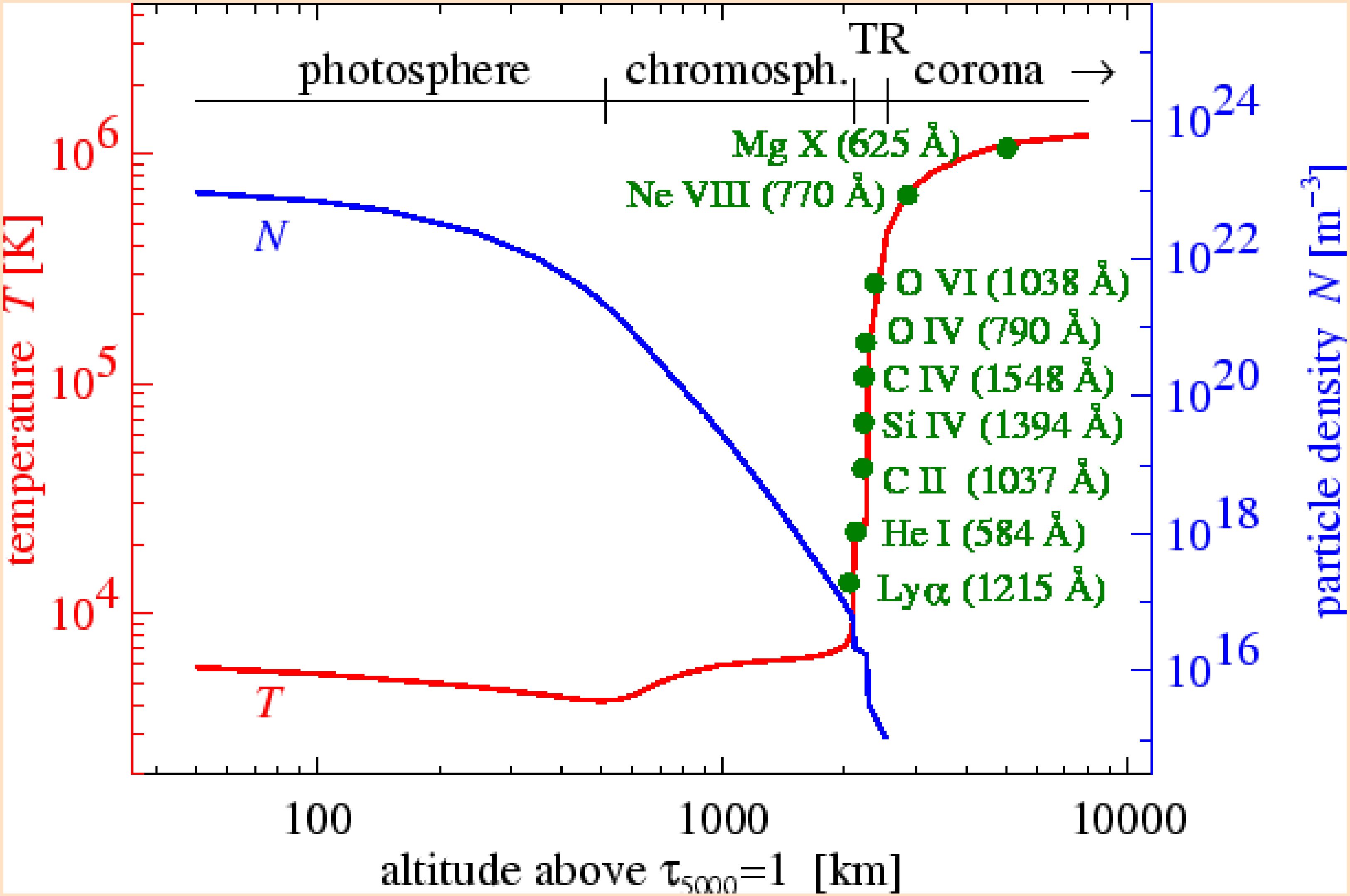

Empirical model of the solar atmosphere (Credit: Hardi Peter)

Emission Lines

$$X_j^{+m} \rightarrow X_i^{+m} + h\nu_{ji}$$

Radiant power density of a spectral line:

$$\varphi(\lambda_{ji}) = N_j(X^{+m})\, A_{ji}\, \Delta\varepsilon_{ij}$$

$$N_j(X^{+m}) = \frac{N_j(X^{+m})}{N(X^{+m})} \frac{N(X^{+m})}{N(X)} \frac{N(X)}{N(H)} \frac{N(H)}{N_e} N_e$$

Irradiance of a spectral line at r:

$$E(\lambda_{ji}) = \frac{1}{4\pi r^2} \int_V \varphi(\lambda_{ij})\, dV$$

For spatially-resolved observations, relevant volume element dV is seen under a certain solid angle element ,

$$d\Omega = \frac{dS}{r^2}$$

where dS is the projected area of dV.

Radiance of a Line:

$$L(\lambda_{ji}) = \frac{\mathrm{d}E(\lambda_{\mathrm{ji}})}{d\Omega} = \varphi(\lambda_{ji})\,\frac{\mathrm{dV}}{4\pi dS}$$

(independent of r from which observation is made).

Averaged radiant power density:

$$\langle \varphi(\lambda_{\mathrm{ji}}) \rangle = \frac{1}{\mathrm{s}} \int_{\mathrm{s}} \varphi(\lambda_{\mathrm{ji}})\,\mathrm{ds}$$

&

$$L(\lambda_{\mathrm{ji}}) = \langle \varphi(\lambda_{\mathrm{ji}}) \rangle \frac{\mathrm{s}}{4\pi}$$

Coronal Model Approximation

$$N_g(X^{+m})\,\mathrm{N^e}\,\mathrm{C^e_{gj}} = \mathrm{N_j}\,\mathrm{A_{ig}}$$

If $A_{jg} >> \mathrm{N_e}\,\mathrm{C^e_{gj}}$ **, then** $N_g(X^{+m}) / \mathrm{N(X^{+m})} \approx 1$

For a typical EUV transition in Fe^{13+}, at coronal density and temperature,

$\mathrm{A_{ig}} \approx 10^{10}\,\mathrm{s^{-1}}$, *whereas* $\mathrm{N_e c^g_{gj}}$ is $\sim 1\mathrm{s^{-1}}$.

Radiant flux density for coronal model:

$$\varphi(\lambda_{jg}) = \frac{\mathrm{N}(X^{+m})}{\mathrm{N(X)}}\frac{\mathrm{N(X)}}{\mathrm{N(H)}}\frac{\mathrm{N(H)}}{\mathrm{N_e}}\,\mathrm{C^e_{gj}}\,\Delta\varepsilon_{\mathrm{gj}}\,\mathrm{N_e^2}$$

$$C^e_{ij} = \frac{8.63\,\mathrm{x}\,10^{-6}\,\gamma_{\mathrm{ij}}(\mathrm{T_e})}{\mathrm{T_e^{1/2}}\quad \omega_{\mathrm{i}}}\exp\left(\frac{-\Delta\varepsilon_{\mathrm{ij}}}{\mathrm{kT_e}}\right)$$

for a Maxwellian electron velocity distribution,

where $$\gamma_{\mathrm{ij}}(\mathrm{T_e}) = \int_0^\infty \Omega_{ij}\exp\left(\frac{-\varepsilon_{\mathrm{ij}}}{\mathrm{kT_e}}\right)\mathrm{d}\left(\frac{\varepsilon_{\mathrm{j}}}{\mathrm{kT_e}}\right)$$

Collision strength $\Omega_{\mathrm{ij}} = \Omega_{\mathrm{ji}}$ $\Rightarrow$ a symmetric and dimensionless quantity &

ε_{j} $\rightarrow$ energy of scattered electron.

For transitions $\Delta\varepsilon_{\mathrm{ij}} << \mathrm{kT_e}$, proton collisional excitations and de-excitations must be considered

[e.g., Fe XIV in ground configuration: $3s^2 3p(^2P_{1/2} - ^2P_{3/2})$**]**

Ionization Balance:

$$N^{+m}(q_{col} + q_{\mathrm{au}} + q_{\mathrm{ct}}) = \mathrm{N}^{+\mathrm{m}+1}(\alpha_r + \alpha_{\mathrm{d}} + \alpha_{\mathrm{ct}})$$

Radiative Recombination:

$$X_n^{+m+1} + \mathrm{e} \rightarrow \mathrm{X}_{\mathrm{n'}}^{+\mathrm{m}} + \mathrm{h}\nu$$

(*Inverse process photoionization not dominant for TR and coronae of stars*)

Di-electronic Recombination:

$$X_n^{+m+1} + \mathrm{e} \rightarrow (\mathrm{X}_{\mathrm{n'}}^{+\mathrm{m}})^{**} \rightarrow \mathrm{X}_{\mathrm{n''}}^{+\mathrm{m}} + \mathrm{h}\nu$$

(*dominant recombination mechanism at high temperatures*)

Emission Measure

$$\varphi(\lambda_{jg}) = \frac{N(X)}{N(H)} \frac{N(H)}{N_e} G(T, \lambda_{jg}) \Delta\varepsilon_{gj} N_e^2$$

where $G(T, \lambda_{jg}) = \frac{N(X^{+m})}{N(X)} C_{gj}^{e}$ ⟶ **contribution function.**

Radiance:

$$L(\lambda_{jg}) = \frac{1}{4\pi} \frac{N(X)}{N(H)} \frac{N(H)}{N_e} \Delta\varepsilon_{gj} \langle EM \rangle \langle G(T) \rangle$$

where $\langle G(T) \rangle = \frac{1}{\Delta T} \int_{\Delta T} G(T, \lambda_{jg})\, dT$.

Emission Measure for spatially-resolved structures: $\langle EM \rangle = \int_{s} N_e^2\, ds$.

Average N_e is crudely deduced: $\langle N_e^2 \rangle = \langle EM \rangle / s$.

Spectral Line Profiles

Line Broadenings ⟶ Dynamic Nature ⟶ TR spectra characterized by broadened line profiles.
Nature of excess broadening ⟶ constraints on heating processes ⟶ Information on wave propagation.

Lines from optically-thin plasmas fitted with Gaussian profiles → Spectral radiance:

$$L_\lambda = \frac{1}{\Delta\lambda\sqrt{\pi}} \exp(-(\lambda - \lambda_0)^2/(\Delta\lambda)^2)$$

$$L(\lambda_0) = \int L_\lambda d\lambda$$

Line radiance at λ_0 with $\Delta\lambda$ Doppler width:

$$(\Delta\lambda)^2 = \frac{\lambda_0^2}{c_0^2}\left(\frac{2kT_i}{M} + \xi^2\right) + \Delta_I^2$$

for a Maxwellian velocity distribution of the ion temperature → $T_i \approx T_e$,

M ⟶ ion mass,

Δ_I ⟶ Gaussian instrumental width &

ξ ⟶ most probable non-thermal velocity.

Comprehensive Reviews
Part I & Part II

Wilhelm, ***Dwivedi***, Marsch & Feldman (2004) ***Space Science Reviews*** **111**, pp. 415 - 480. **Part I**

Wilhelm, Marsch, ***Dwivedi*** & Feldman (2007) ***Space Science Reviews*** **133**, pp. 103 – 179. **Part II**

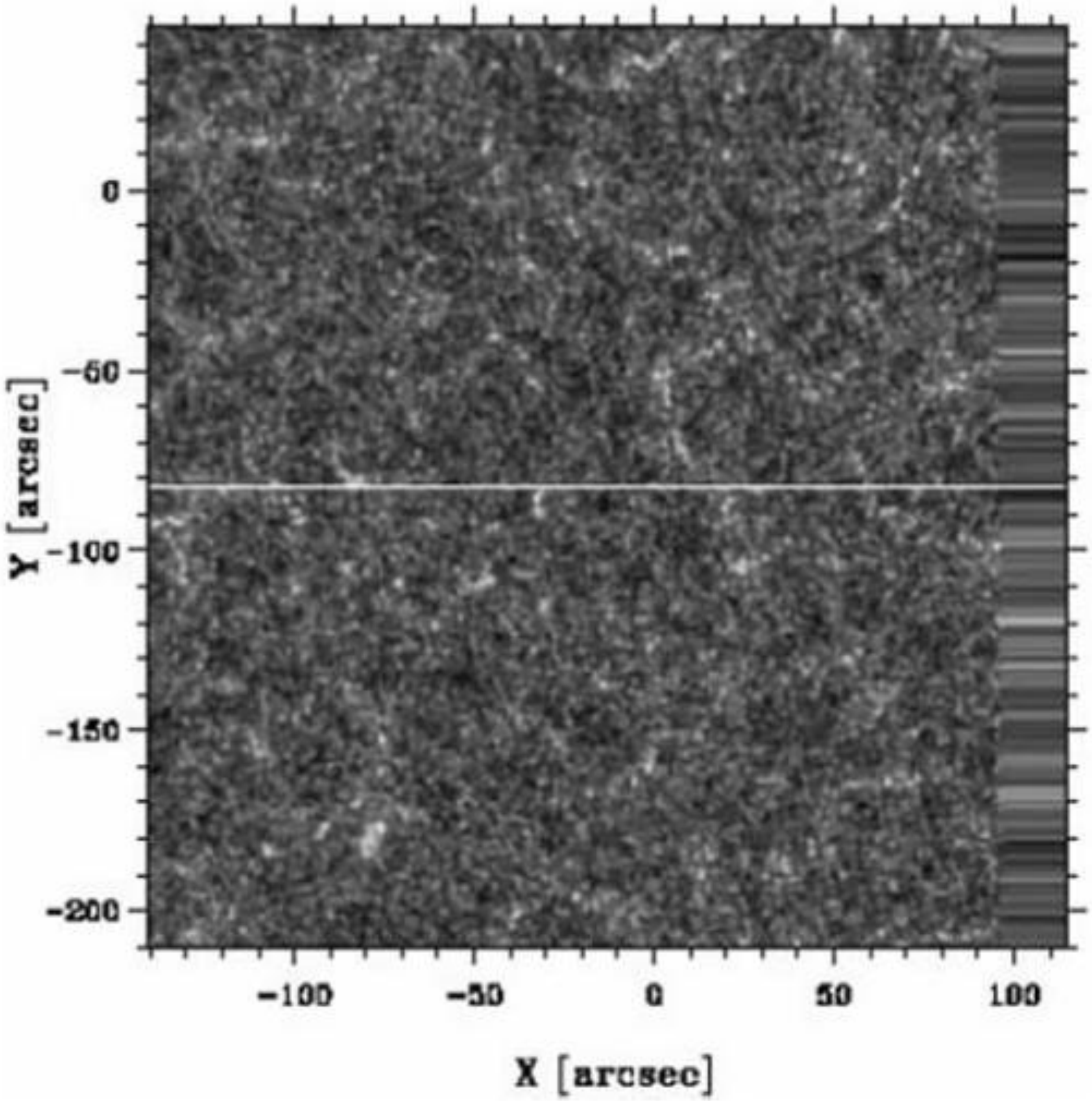

Upper photosphere of the quiet Sun from TRACE in 170 nm passband (Krijger *et al.* 2001).

Chromospheric network lanes as an ensemble of discrete dots in brightness but also many tiny bright points (≈ 1 Mm) called grains in the inter-network area.

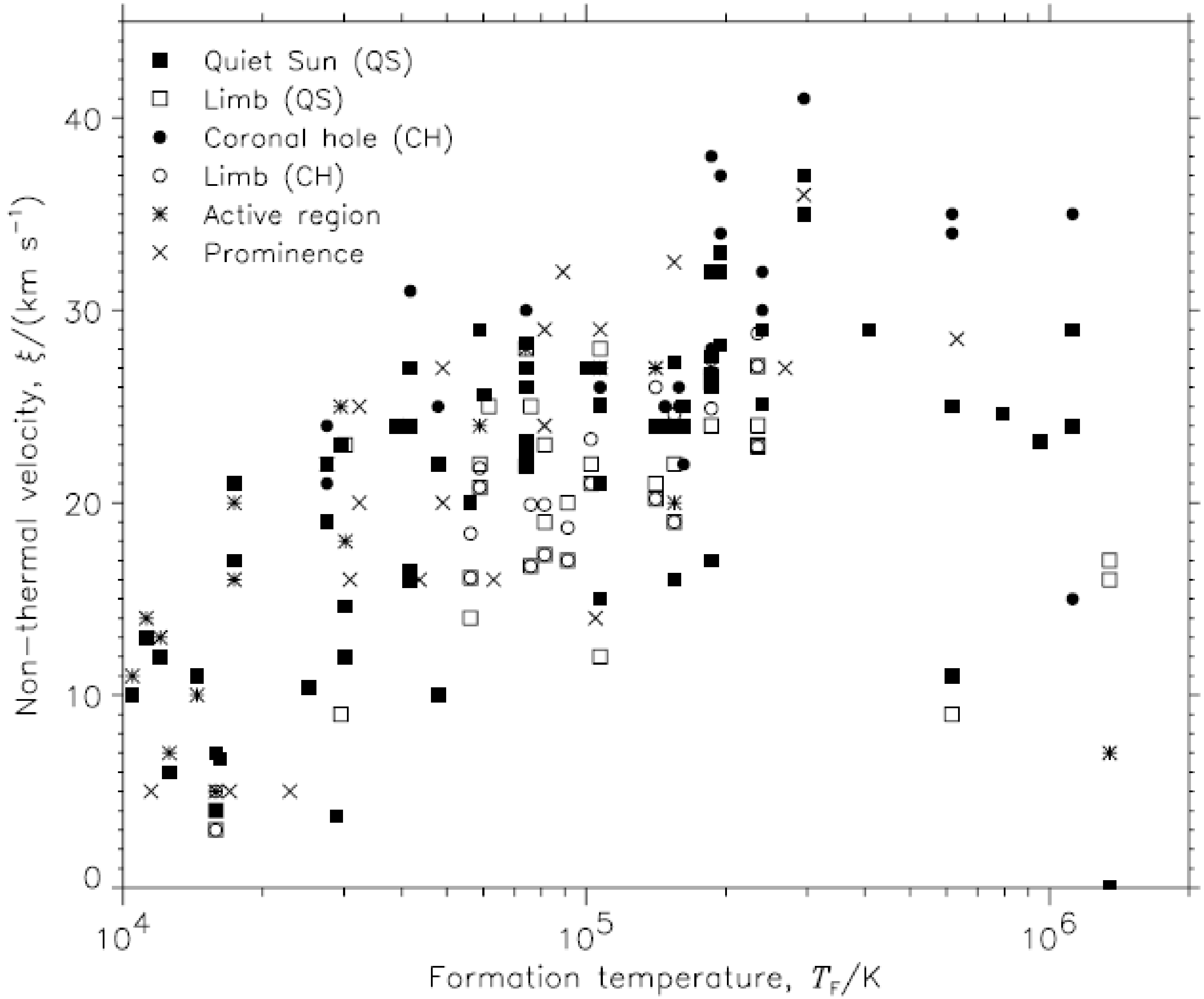

Nonthermal ion velocities (turbulent speeds) from spectral line widths as a function of formation temperature observed on the disk by several instruments under varying plasma conditions from chromosphere to TR and corona (Wilhelm *et al.* 2004).

No systematic differences in ξ → ξ ≈ 10 km/s in chromosphere, turbulence increases (> 10 km/s) in TR (< 2x10⁵ K).

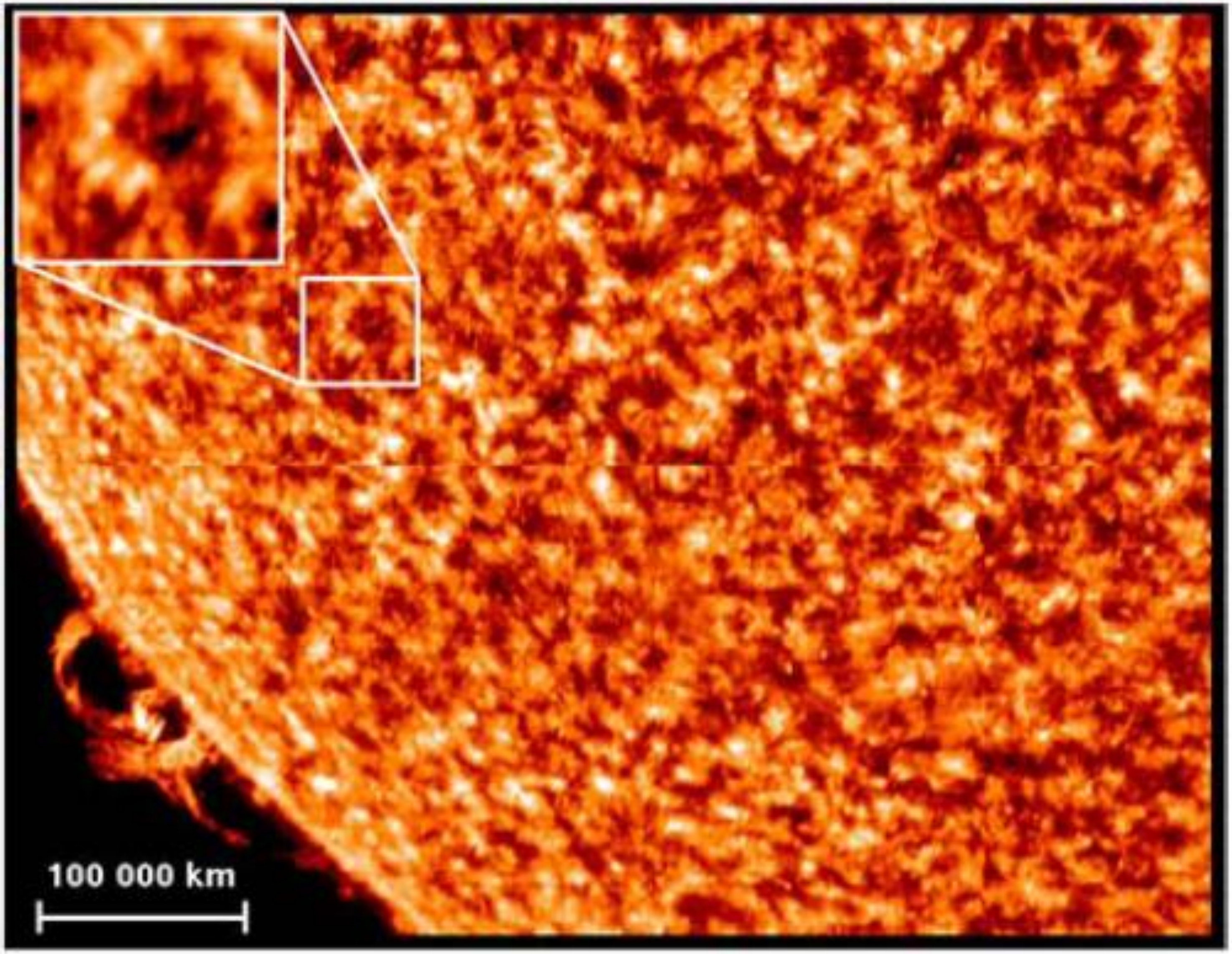

TR seen in C III VUV emission line. Various structures are visible → Network cells being most conspicuous. Blown up cell with small loops bridging the network lane.

Exemplary image of magnetic network in C III.

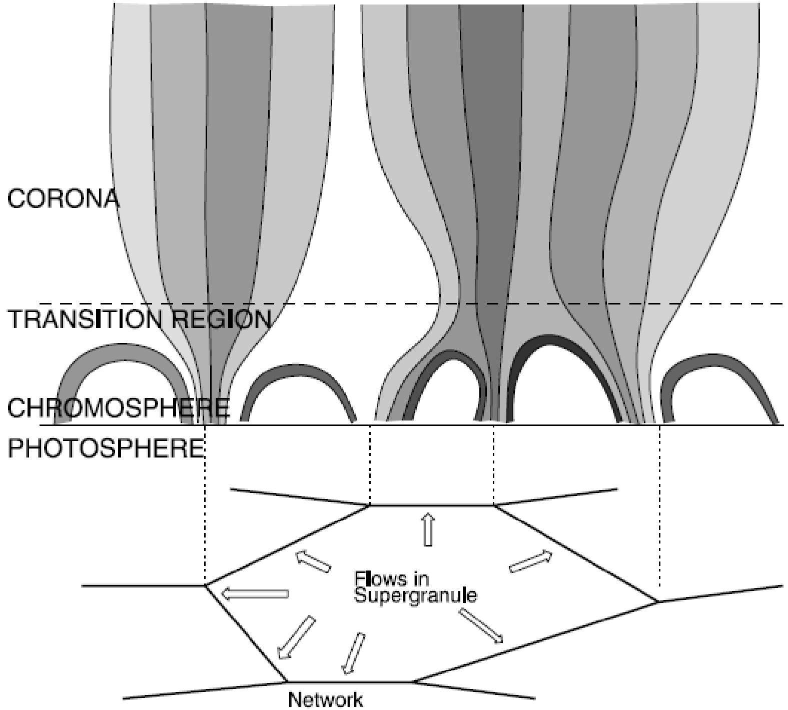

Building blocks of the magnetic network with its main structures → closed loops and open funnels.
The fields originating in the network lanes may be open or close → covering supergranulation cells or providing magnetic flux to the upper corona (Aschwanden 2004)

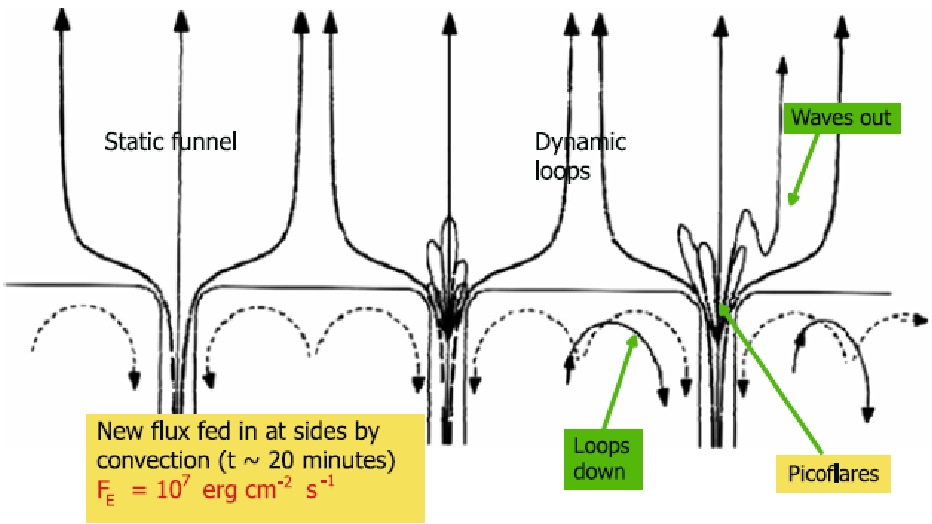

Dynamic network as a wave and turbulence generator through convection-driven reconnection (Axford & McKenzie 1997)

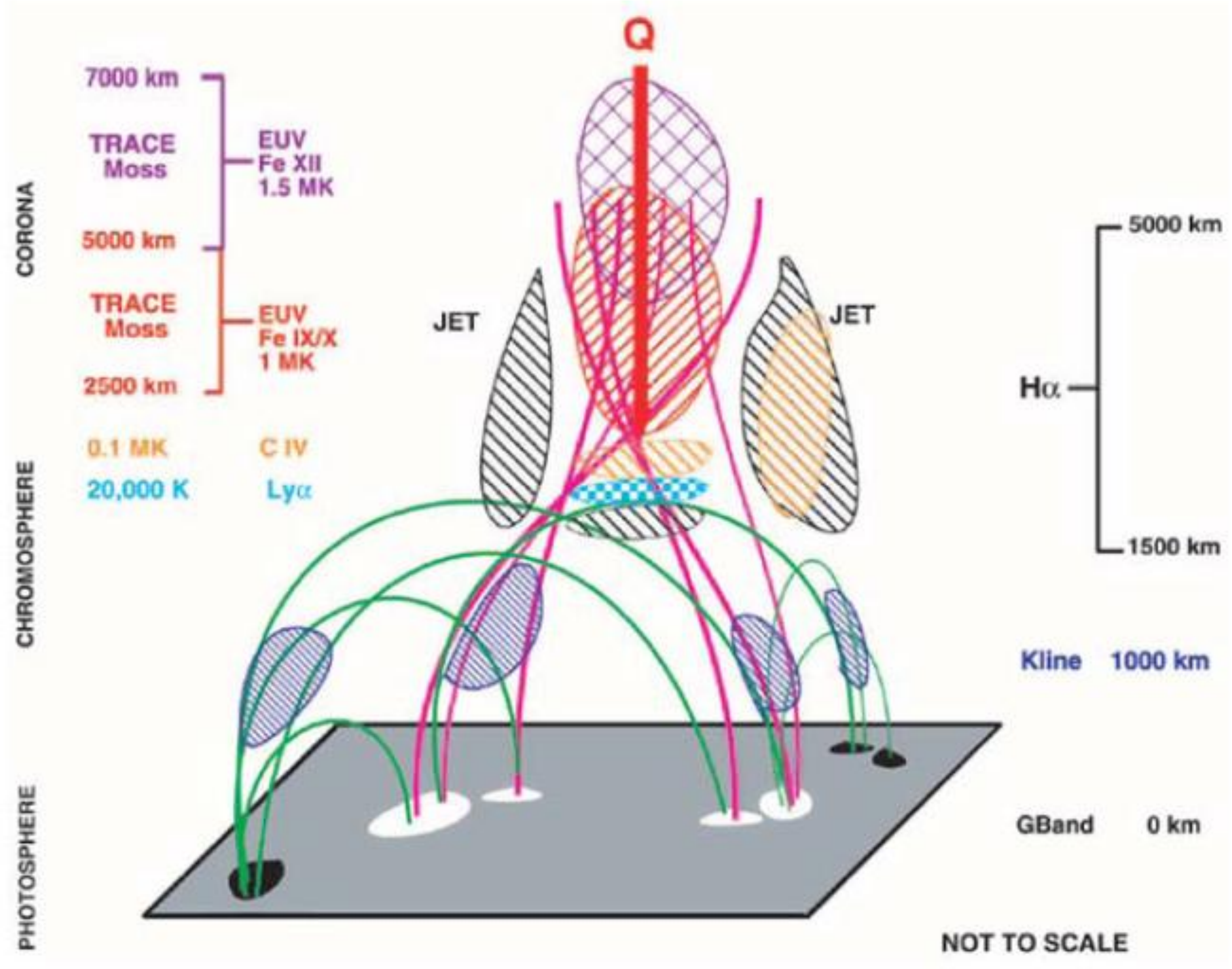

TR with various emission regions and magnetic structures (De Pontieu et al. 2003).

Various dynamic features of the magnetic TR vis-à-vis classical temperature TR.

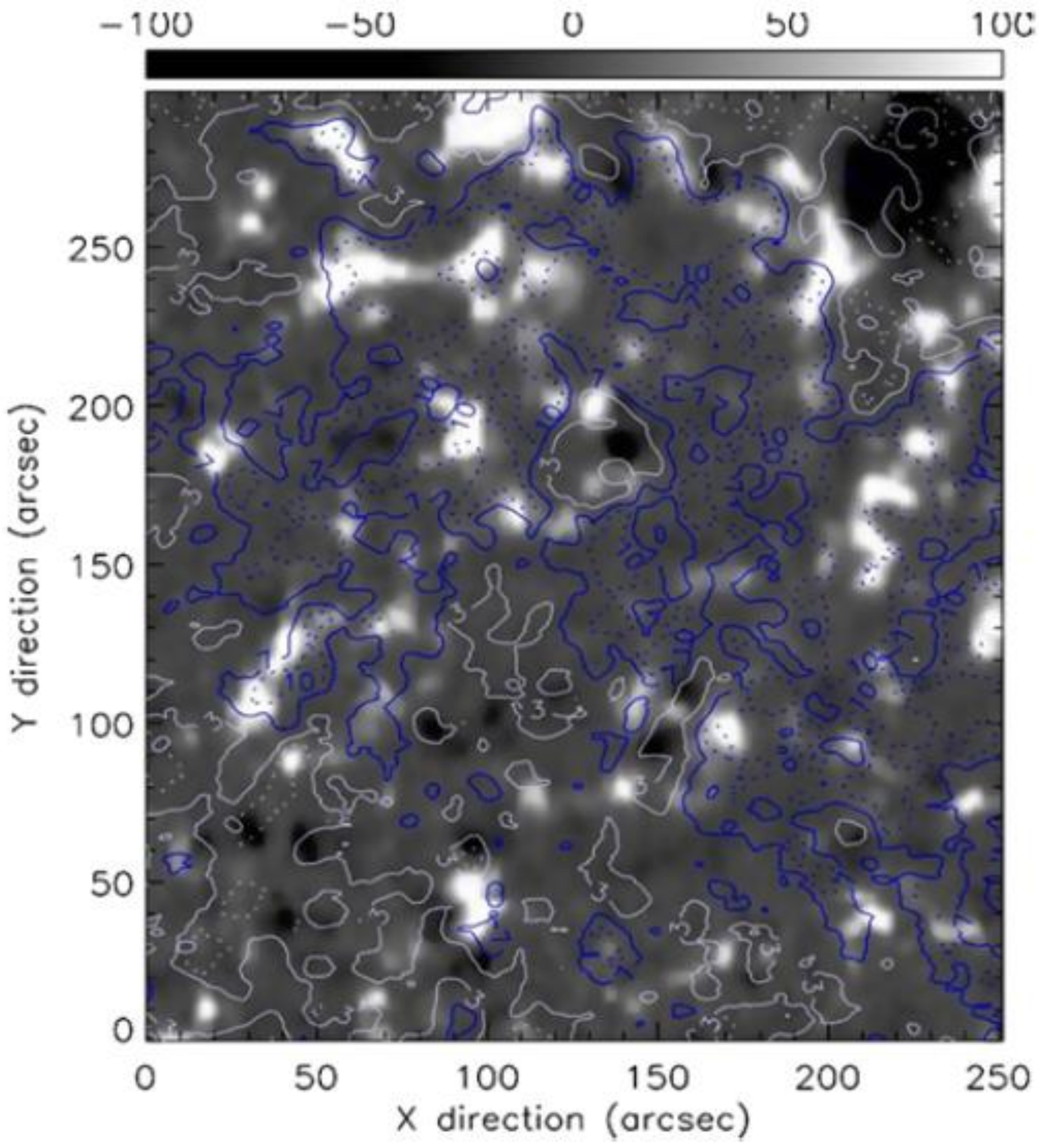

Blue contours: dotted 10 km/s, solid 7 km/s.

White contours: dotted 0 km/s, solid 3 km/s.

KPNSO magnetogram:

White – positive polarity

Black – negative polarity

The **grey scale** ranges from -100 G to 100 G.

Photospheric magnetogram and Ne VIII (77 nm) outflow → SUMER observations of Doppler blue shifts. (Xia *et al.* 2003)

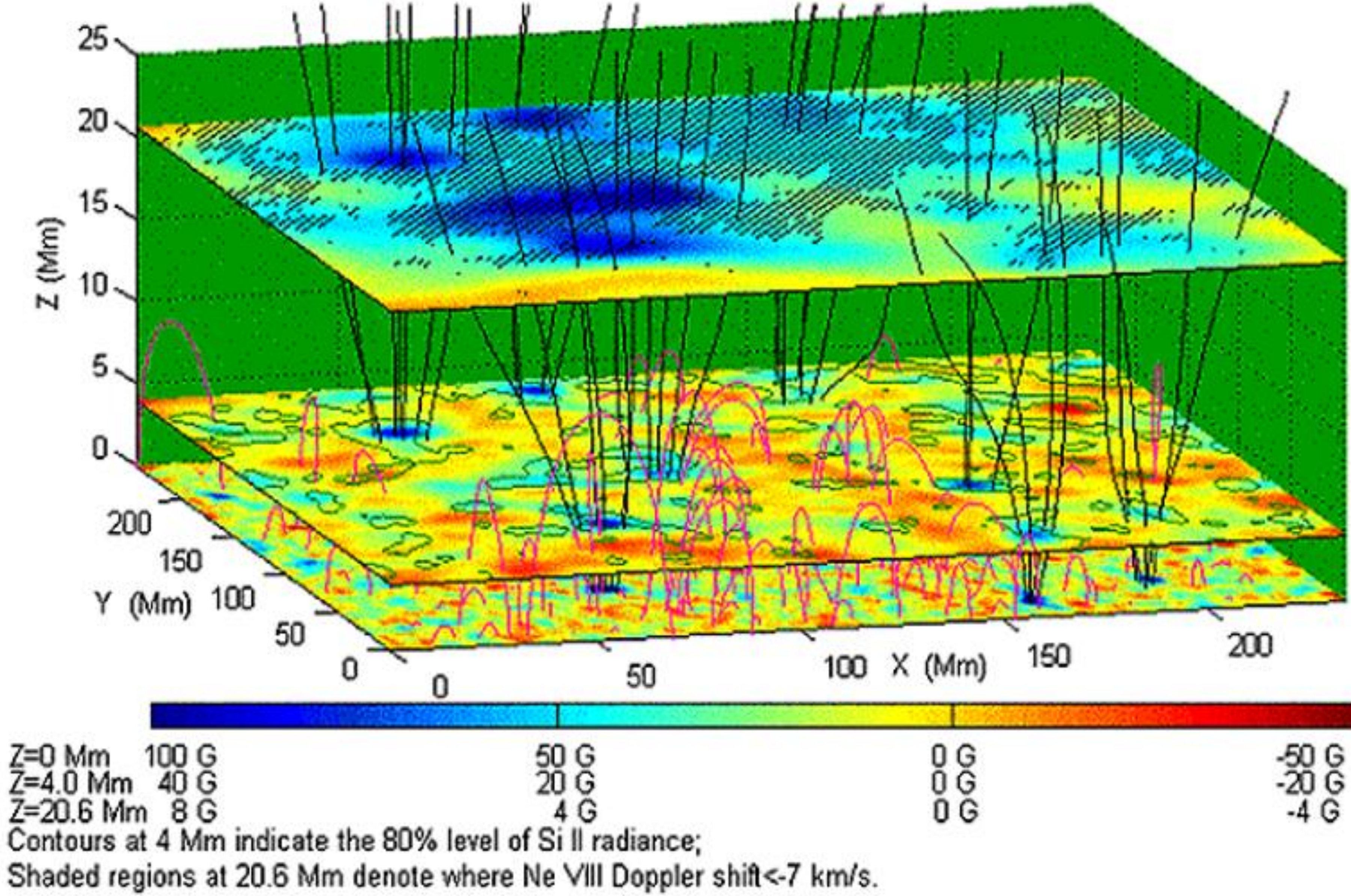

Source regions of the fast solar wind in the magnetic funnels of a coronal hole. The magnetic field magnitude is shown at 4 Mm and 20 Mm (Tu *et al*. 2005).

Physically consistent model for Magnetic TR → Demonstration of coronal heating via Reconnection (at ~ 5 Mm) → Possible by anomalous resistivity (via current-driven micro-instabilities).

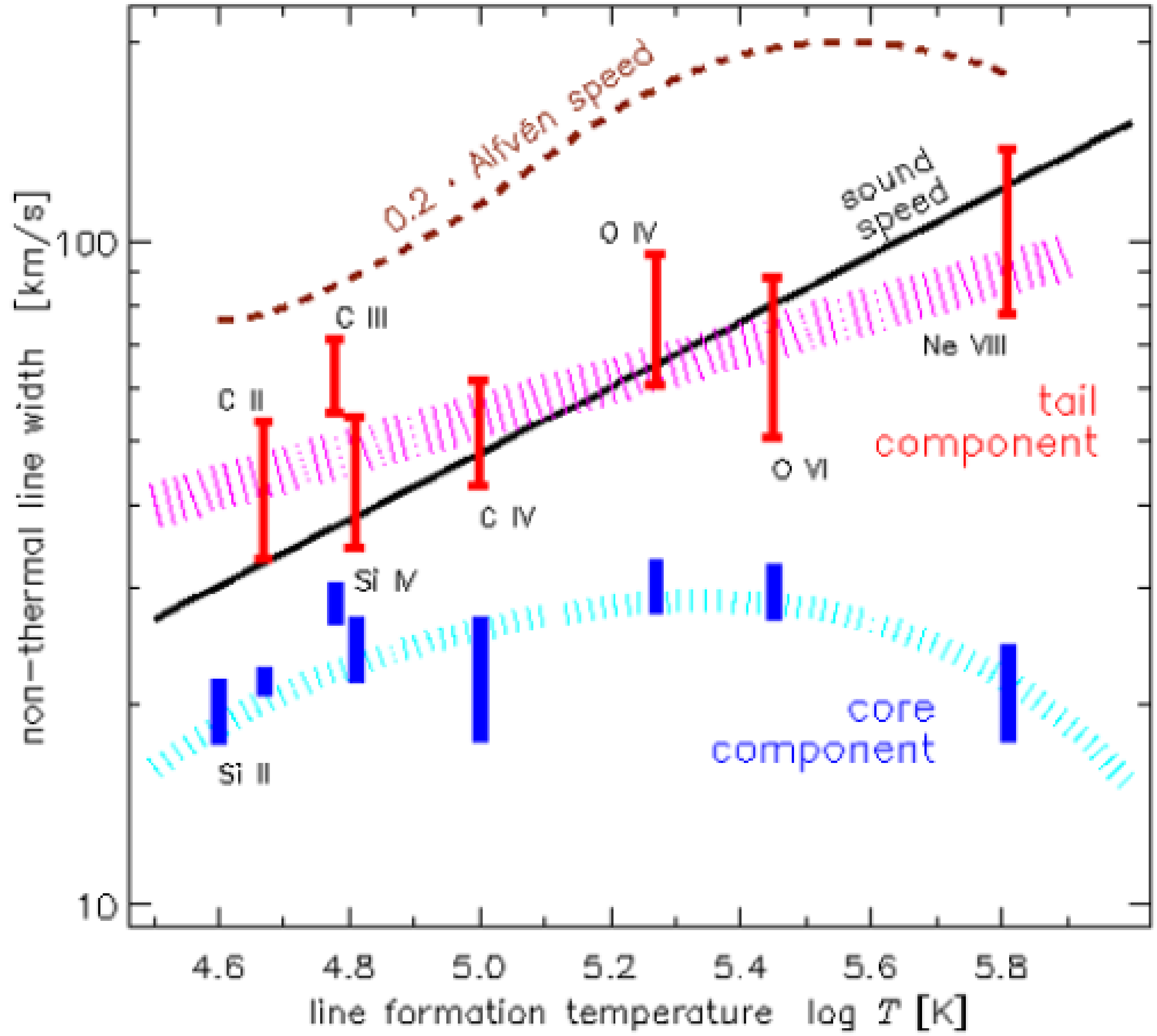

Emission line widths as a function of height in the lower corona (Peter 2001)

A clear separation in line width between core and tail components:

20 – 30 km/s in core but growing with height from ~ 40 to 90 km/s in line tail.

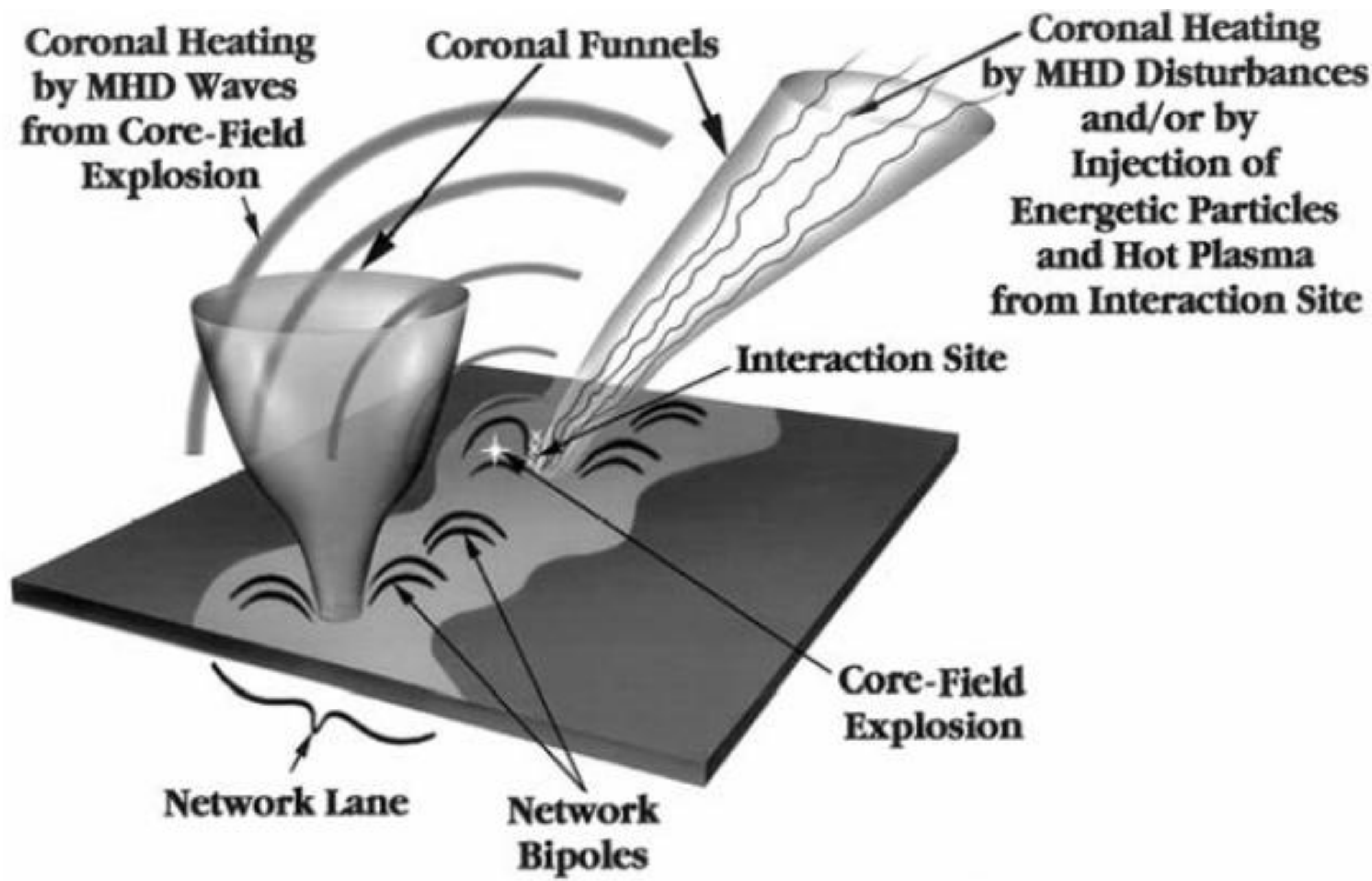

Scenario for heating the corona in quiet regions and coronal holes by core-field explosions in network bipoles (Moore *et al.* 1999)

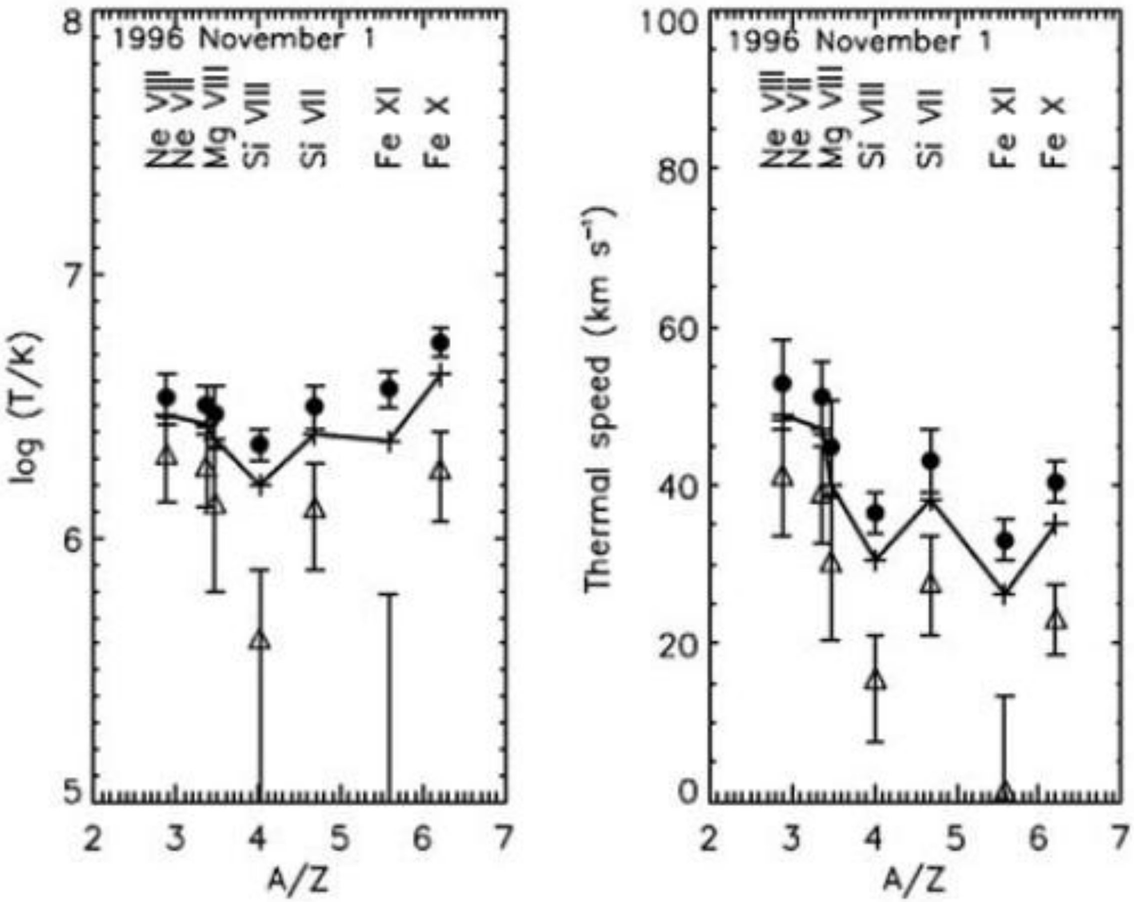

Minor ion temperatures and thermal speeds in a southern coronal hole.

Left: Common logarithm of ion temperature *vs* A_i/Z_i ratio of ions.

Right: Thermal speed of ions.

Full dots → ξ km/s; Triangles → ξ = 34 km/s; Solid curves → ξ = 25 km/s.

Uncertainties → ± 0.2 pixel variation of Gaussian fit. (Tu *et al*. 1998)

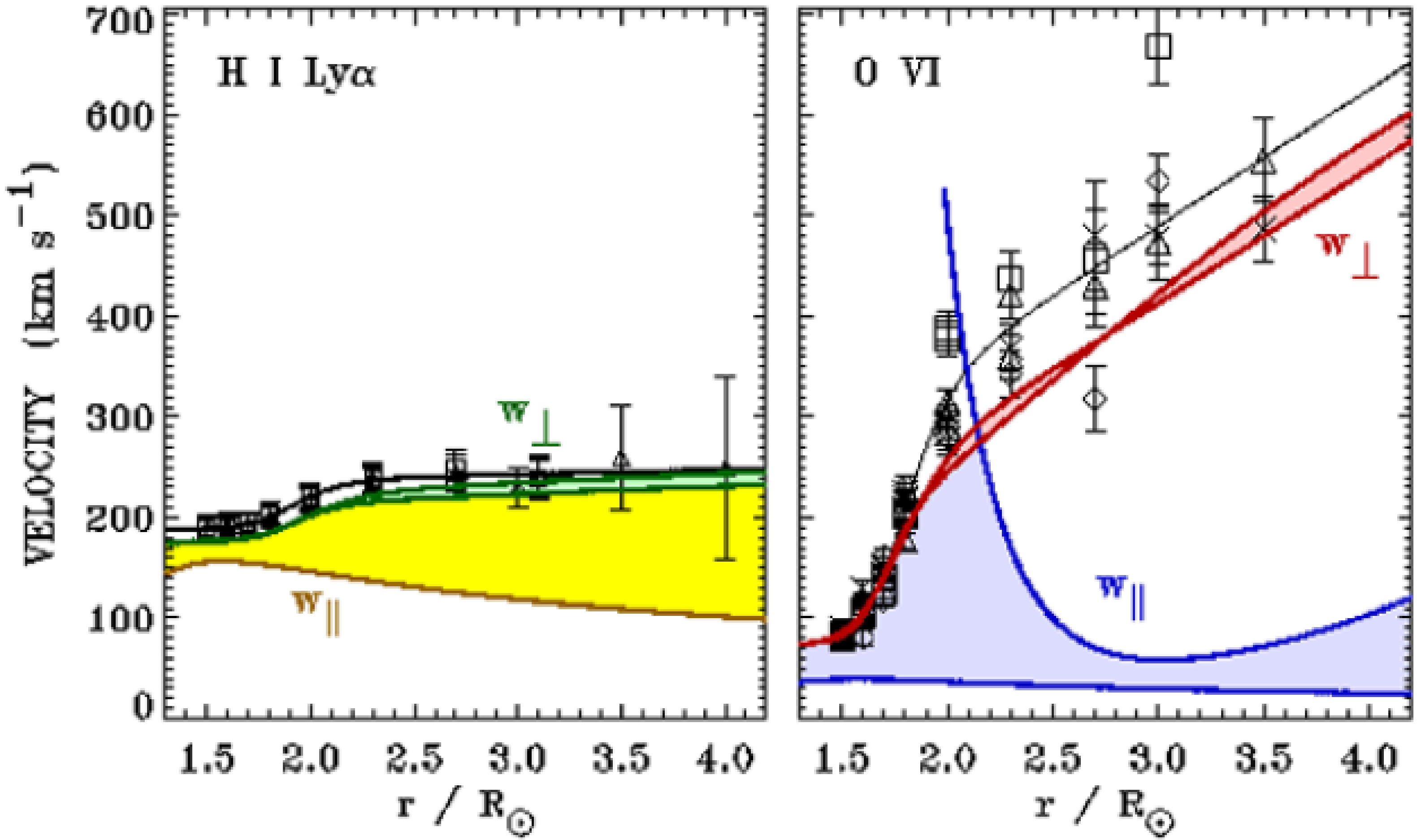

Proton (left) and O^{5+} (right) ion thermal speed perpendicular ($W_{\perp}$) and parallel ($W_{||}$) to magnetic field in a southern polar coronal hole.

N.B.: ***Pronounced preferential heating of oxygen with respect to protons $\Rightarrow$ ion-cyclotron heating (Cranmer et al. 1999).***

Elemental Composition

- High-resolution UV & X-ray spectra provide access to coronal abundances (essentially C, N, O, Ne, Mg, Al, Si, S, Ar, Ca, Fe, Ni etc.)

- Coronal plasmas are generally optically thin.

- Do coronal abundances in the Sun and stars reflect the photospheric composition?

First Ionization Potential (FIP), Photospheric & Solar Atmosphere Abundances

Element		Ionization potential (eV)	Photospheric abundance	Log$_{10}$ solar abundance above typical quiet regions	
			Log$_{10}$	$3 \times 10^4 \le T \le 8 \times 10^5$ K	$\sim 1.4 \times 10^6$ K
1	H	13.6	12.00	12.00	12.00
2	He	24.6	10.93	10.93	10.93
6	C	11.3	8.52	8.52	8.52
7	N	14.5	7.92	7.92	7.92
8	O	13.6	8.83	8.83	8.83
10	Ne	21.6	8.11	8.11	8.11
11	Na	5.1	6.32	6.62	6.92
12	Mg	7.6	7.58	7.88	8.18
13	Al	6.0	6.49	6.79	7.09
14	Si	8.2	7.56	7.86	8.16
16	S	10.4	7.33	7.33	7.33
18	Ar	15.8	6.59	6.59	6.59
20	Ca	6.1	6.35	6.65	6.95
26	Fe	7.9	7.50	7.80	8.10
28	Ni	7.6	6.25	6.55	6.85

High-FIP (≥ 10 eV) elements are of photospheric composition, whereas low-FIP (≤ 10 eV) elements are overabundant (e.g., Feldman 1992).

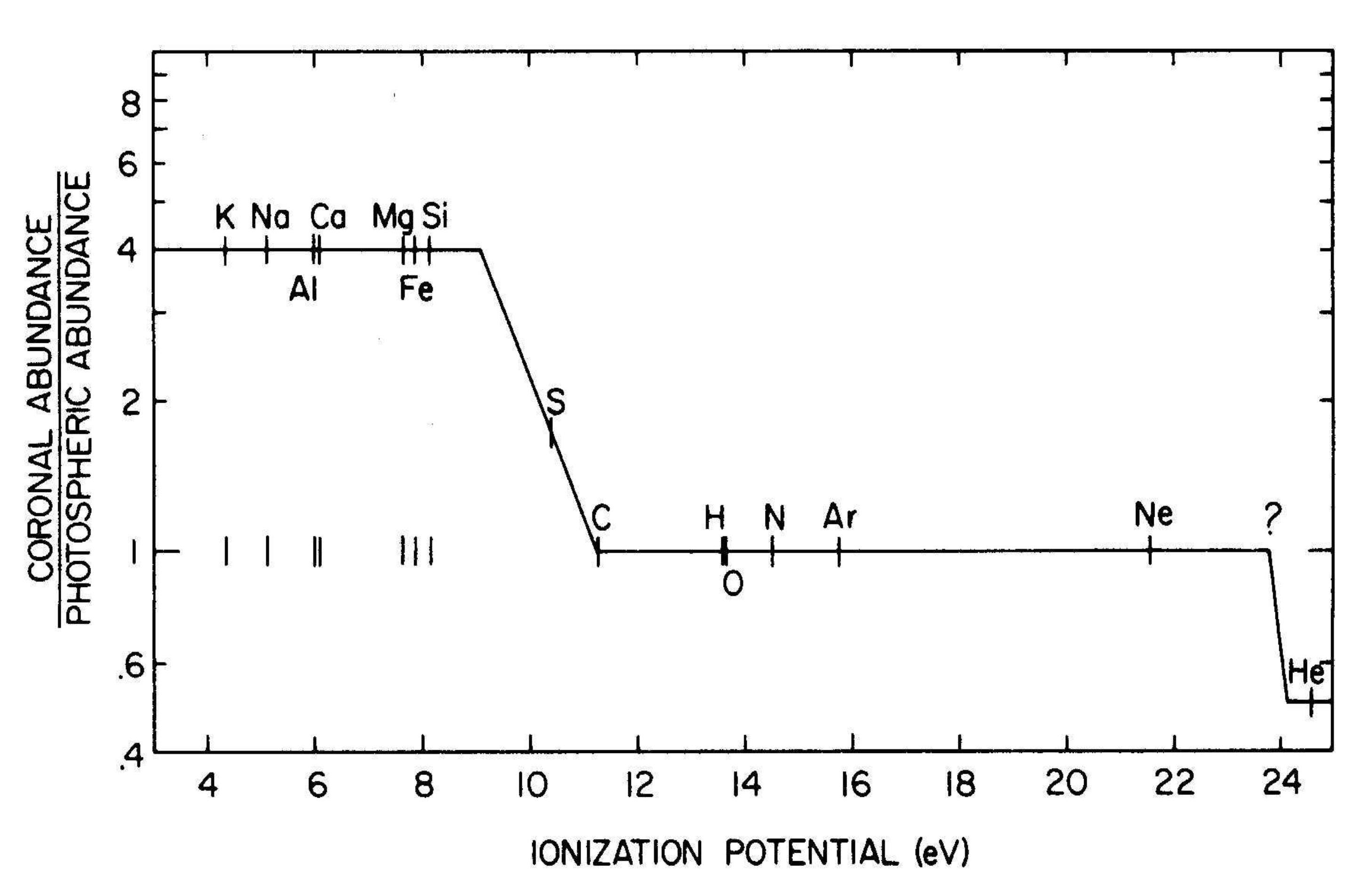

Solar chromosphere: T ≈ 5,000 – 10,000 K ⟶ Ionized low-FIP elements and neutral high-FIP elements.

i. **Fractionation mechanism in chromosphere, &**
ii. **Transportation mechanism into the corona**

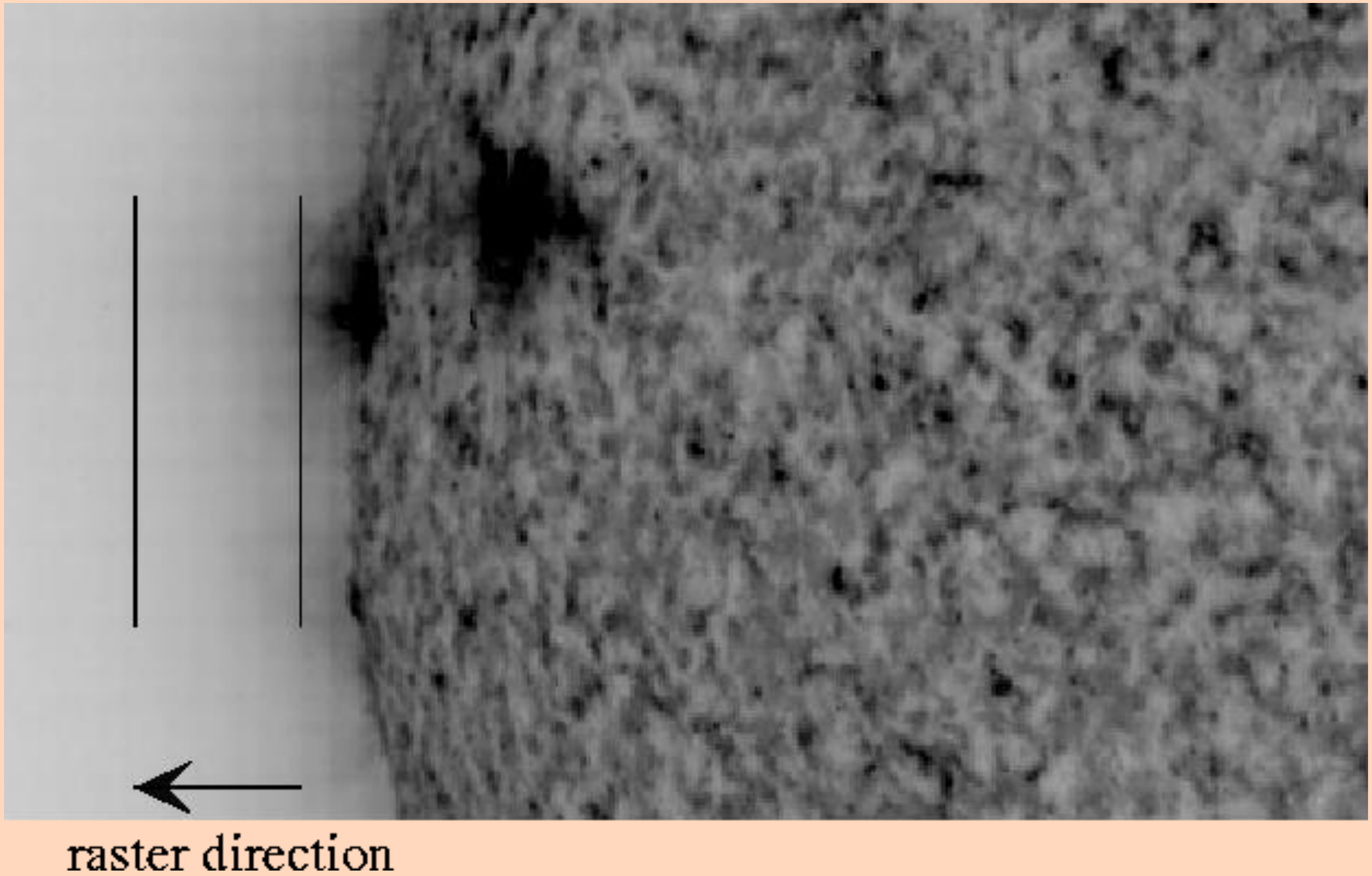

SUMER/*SOHO* raster superimposed on a section of the 304 Å EIT image taken at 19:41 UT, showing the active region NOAA 7974 on the limb and its neighbour NOAA 7973 (Dwivedi *et al.* 1999, 2004)

Spectral Lines

Ion	Wvl. (Å)	Transition
Ne VI	992.73	$2s^2 2p\ ^2P_{1/2} - 2s2p^2\ ^4P_{3/2}$
K XIII	994.58	$2s^2 2p^3\ ^4S_{3/2} - 2s^2 2p^3\ ^2D_{3/2}$
Ne VI	997.14	$2s^2 2p\ ^2P_{1/2} - 2s2p^2\ ^4P_{1/2}$
Ne VI	999.26	$2s^2 2p\ ^2P_{3/2} - 2s2p^2\ ^4P_{5/2}$
Ne VI	1005.70	$2s^2 2p\ ^2P_{3/2} - 2s2p^2\ ^4P_{3/2}$
Ne VI	1010.25	$2s^2 2p\ ^2P_{3/2} - 2s2p^2\ ^4P_{1/2}$
Ar XII	1018.87	$2s^2 2p^3\ ^4S_{3/2} - 2s^2 2p^3\ ^2D_{5/2}$
Mg VII	1189.85	$2s^2 2p^2\ ^3P_1 - 2s^2 2p^2\ ^1S_0$
Mg VI	1190.10	$2s^2 2p^3\ ^4S_{3/2} - 2s^2 2p^3\ ^2P_{3/2}$
Mg VI	1191.64	$2s^2 2p^3\ ^4S_{3/2} - 2s^2 2p^3\ ^2P_{1/2}$
S X	1196.25	$2s^2 2p^3\ ^4S_{3/2} - 2s^2 2p^3\ ^2D_{5/2}$
Si XI	604.17	$2s2p\ ^1P_1 - 2p^2\ ^1D_2$
S X	1213.00	$2s^2 2p^3\ ^4S_{3/2} - 2s^2 2p^3\ ^2D_{3/2}$

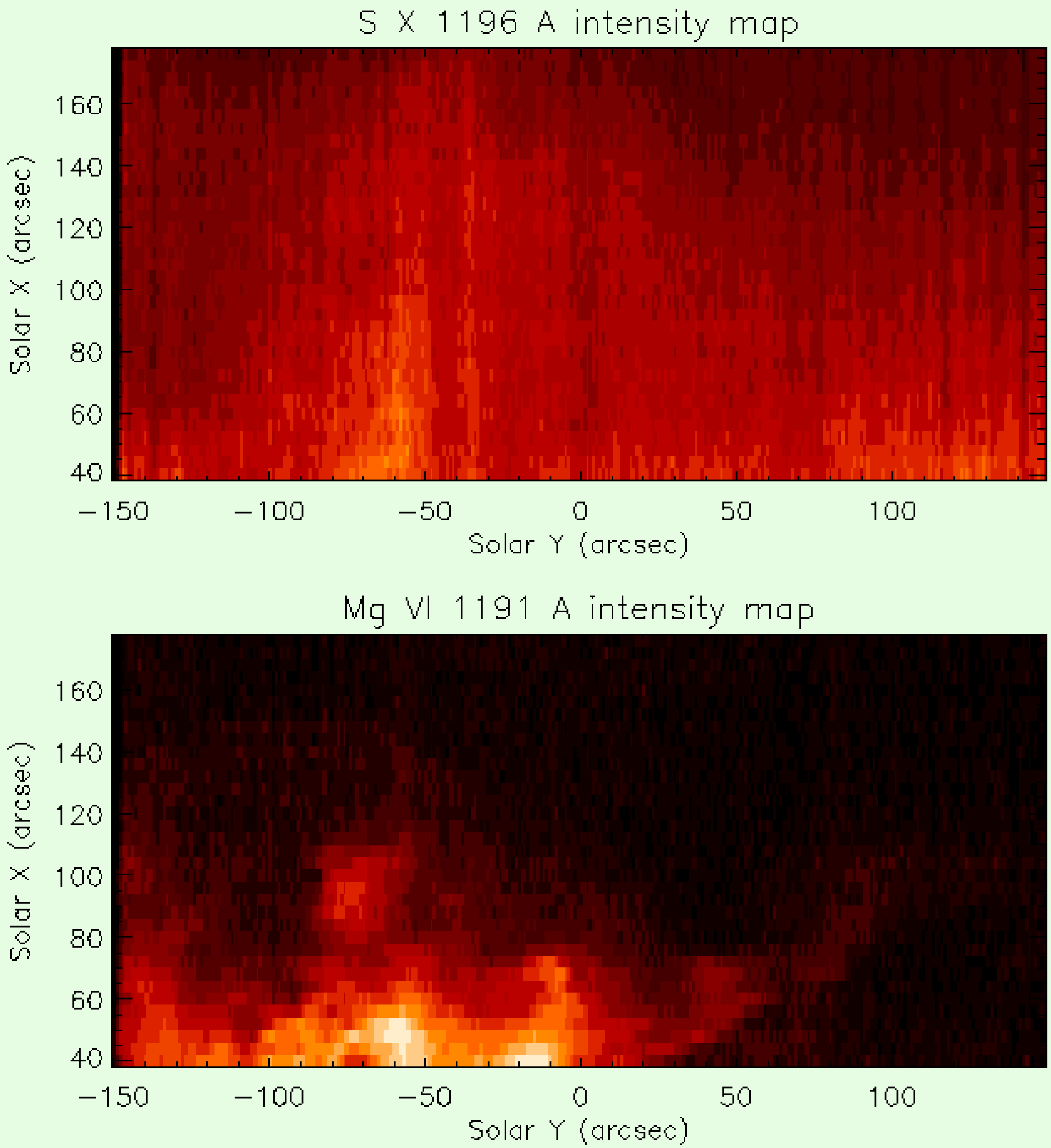

1196 Å (top) and 1191 Å (bottom) intensity maps of the emitting region

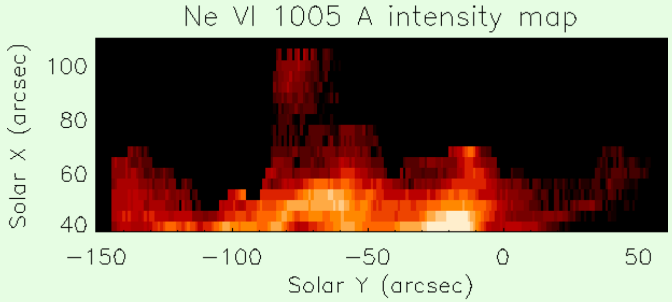

1005 Å intensity map of structures (in black portion line intensity is due mainly to instrument-scattered light)

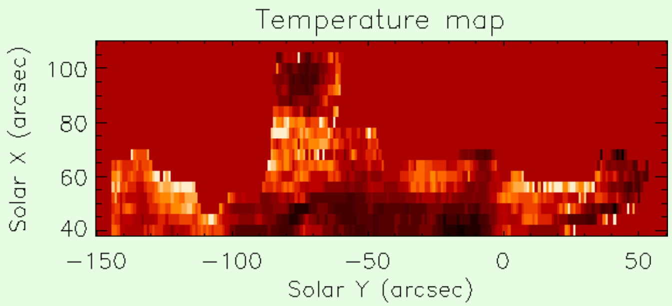

Temperature map from the line ratio

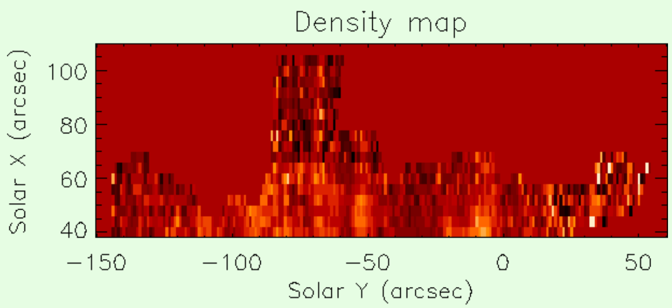

Density map from the line ratio

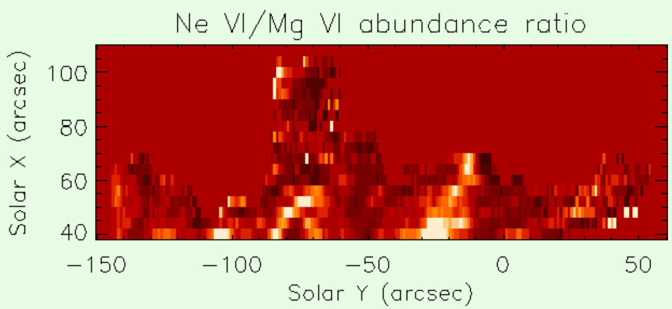

Line ratio, yielding an estimate of the Ne/Mg abundance

Diagnostic results in the active region structures

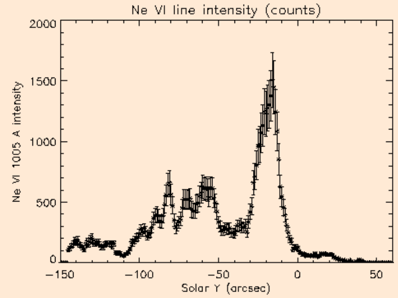

1005 Å intensity

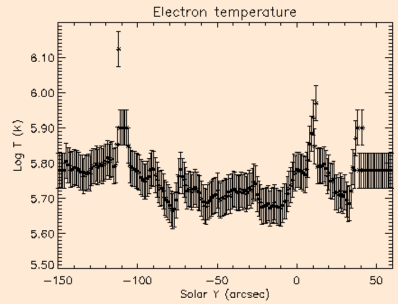

Temperature from the line ratio

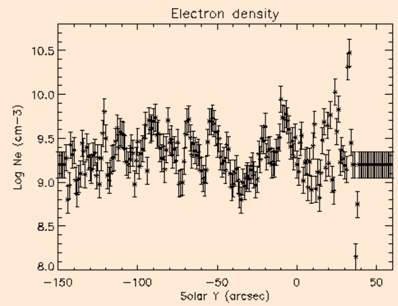

Density from the lie ratio.

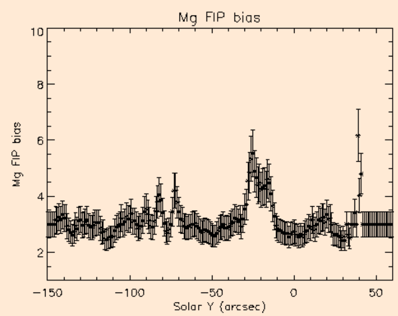

Line ratio, yielding an estimate of the relative Ne/Mg abundance

Diagnostic results in the active region structures, at solar X = 45"

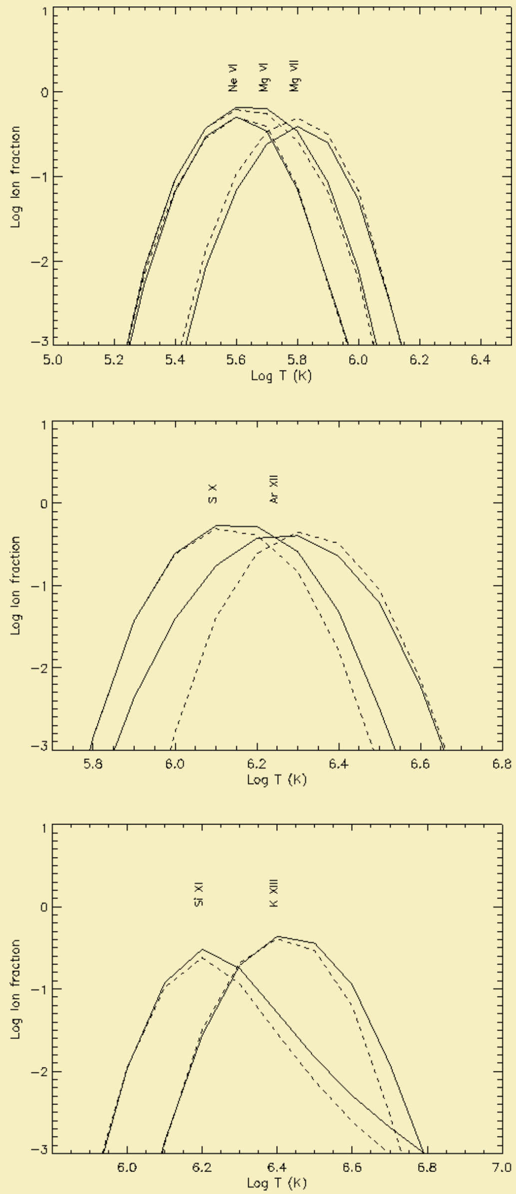

Full line: Mazzotta *et al.* (1998). Dashed line: Arnaud & Rothenflug (1985) (Si, S, Ar), Landini & Monsignori Fossi (1991) (K).

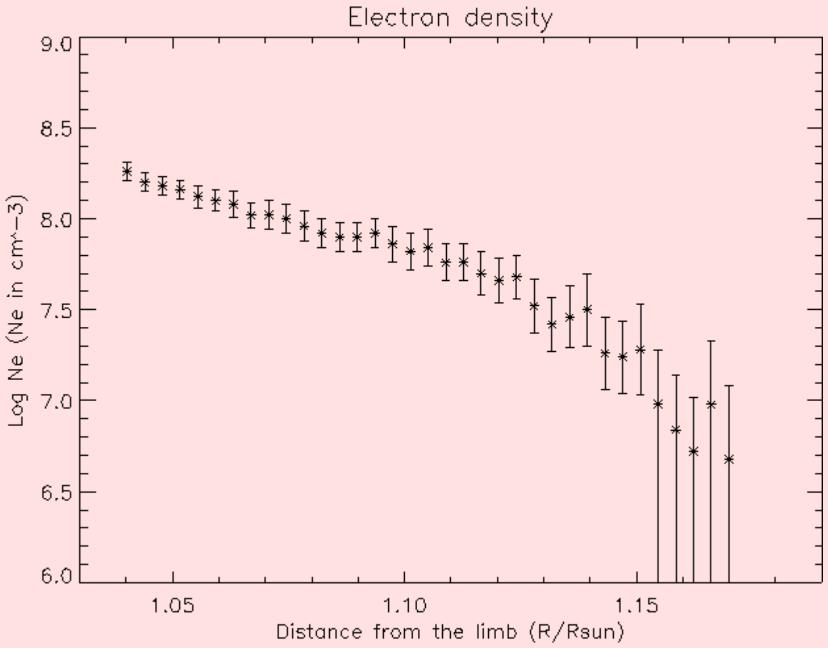

Density *vs* height from line ratio

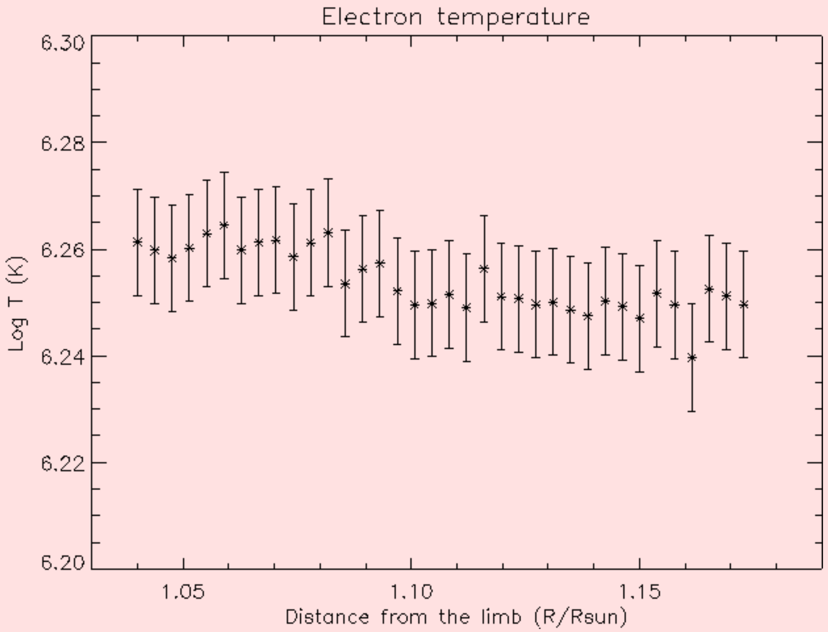

Temperature *vs* height from line ratio

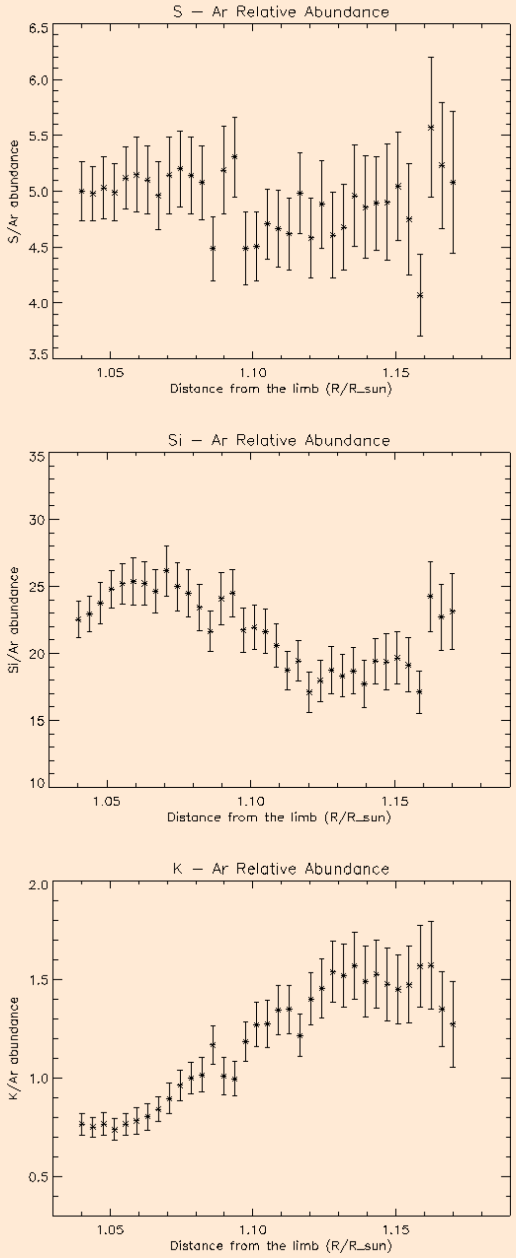

S, Si and K element abundances relative to the Ar photospheric abundance

RESULTS

- **Mg/Ne relative abundance is highly variable in the complex, cool core of the active region, strongly correlated with line intensity and magnetic structures.**
- **Mg abundance enhancements relative to Ne reach up to a factor of 8.8.**
- **In off-limb active region plasma the FIP bias inside elements' class is dependent on the FIP value, being higher for the very-low FIP element K.**
- **The FIP bias versus FIP problem is still open.**

Spectroscopic Diagnostics of Polar Coronal Plumes Observed from Space

(Wilhelm, Dwivedi & Curdt, 2010)

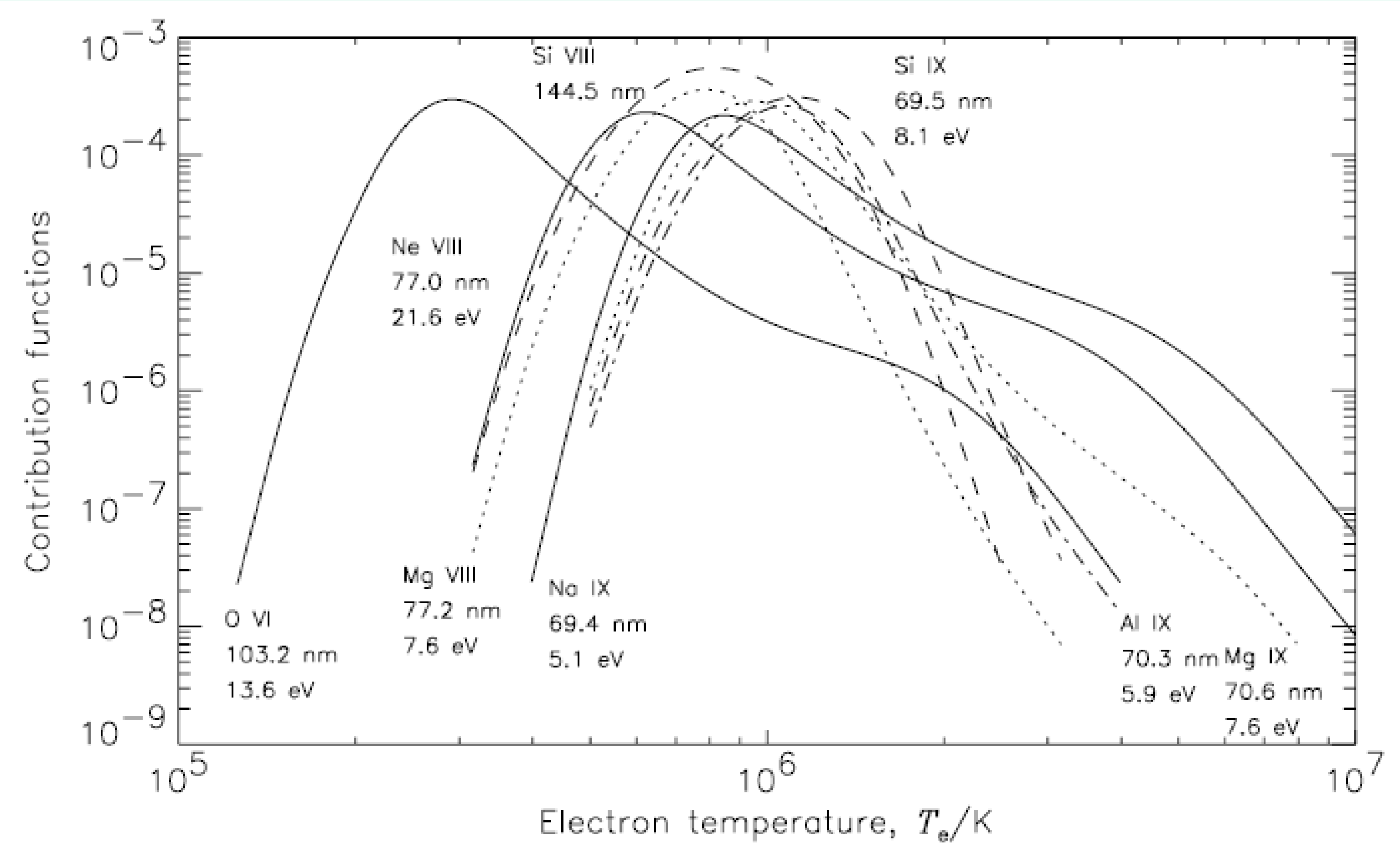

Contribution functions of observed lines and FIP values of corresponding elements

Neon and Oxygen → high-FIP values, whereas other elements → low-FIP biases (< 10 eV)

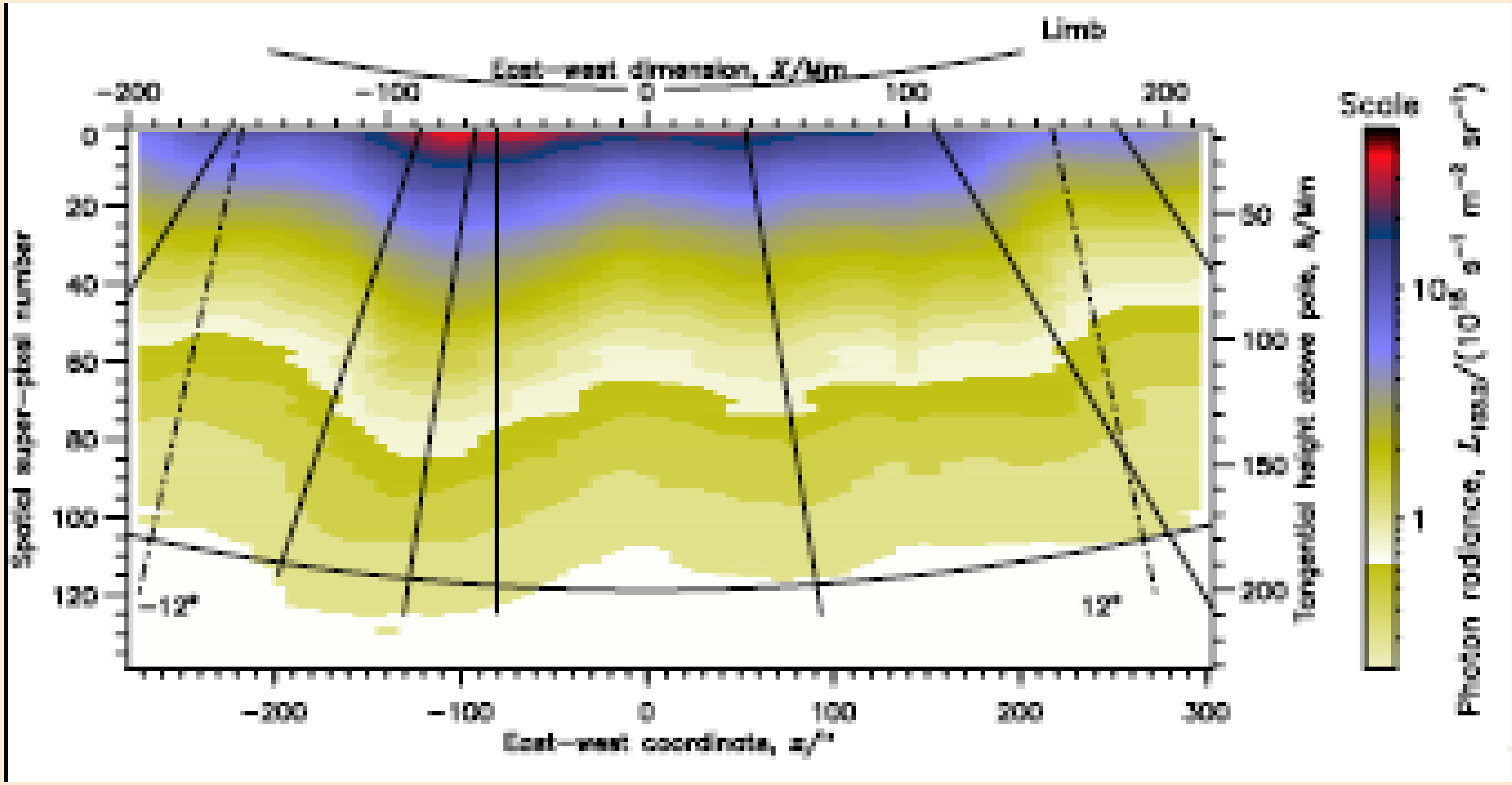

A large raster above the southern CH was obtained in several VUV emission lines. It took 36 h starting on 7 Apr at 01:00 UTC in West-East direction.

The photon radiance of λ1032 O VI is shown here. Radial dashed-dotted lines are shown at 12 off the pole.

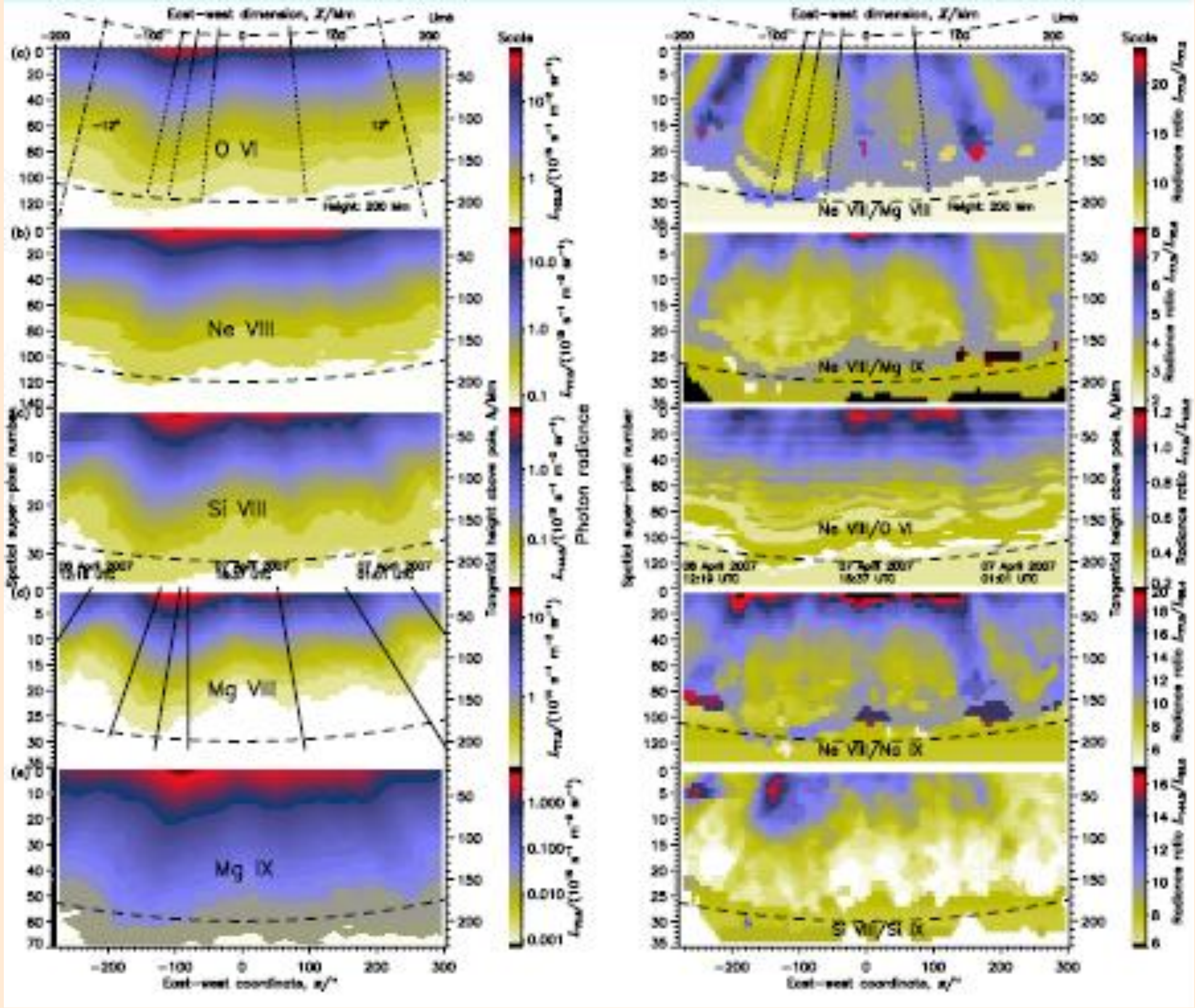

Left: Radiance maps of other observed lines for the same time interval in April 2007. The Na IX line slightly blended by a Mg IX line.

Right: Rato maps of line radiances: O VI, Ne VIII, Si VIII, Mg VIII, Mg IX

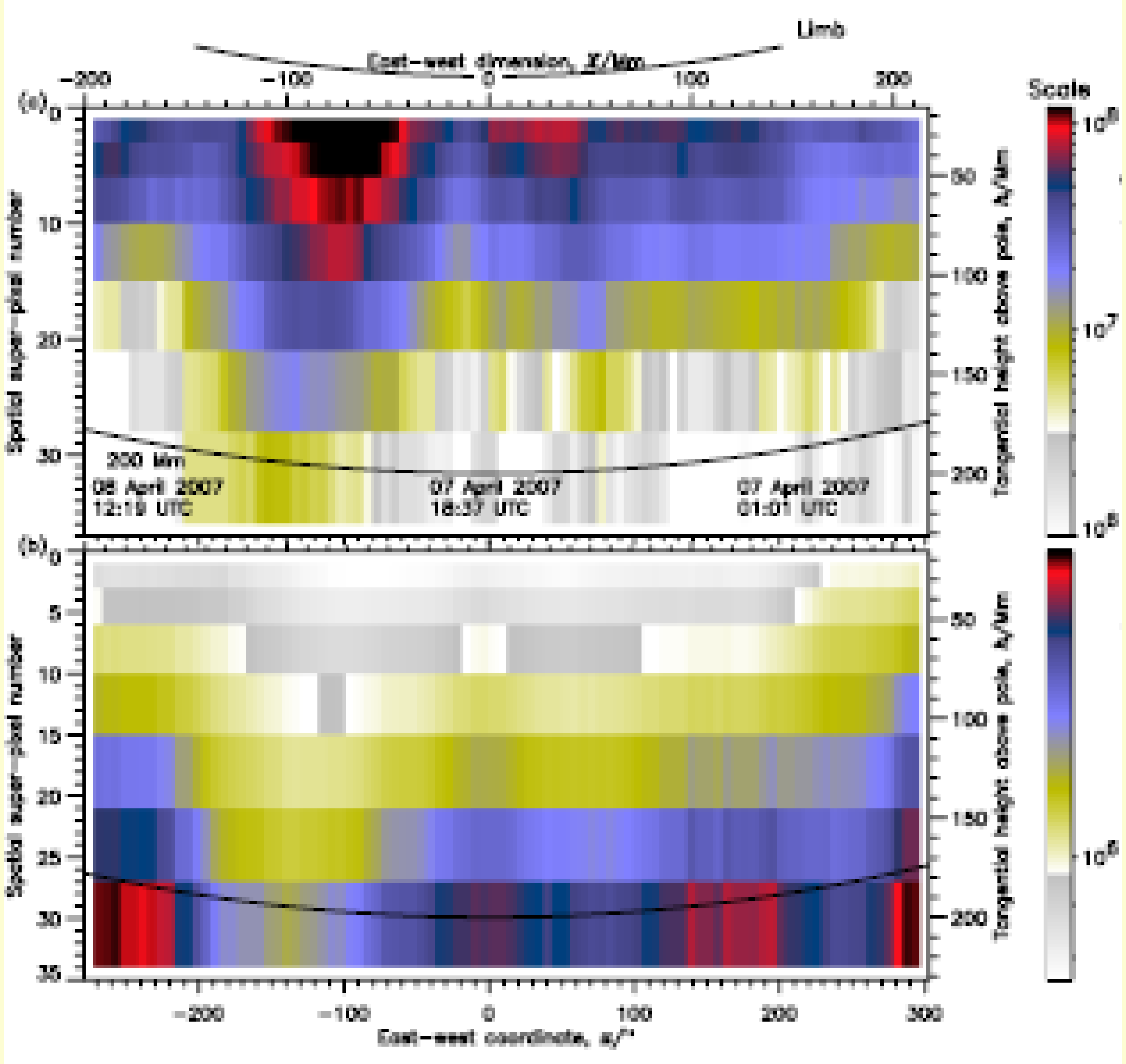

a. Electron density map

b. Electron temperature map

Line ratio Ne VIII /Mg VIII can monitor abundance variations between high-FIP and low-FIP elements.

However, different temperatures in plume and inter-plume regions should be taken into account in view of high-temperature tail of lithium-like Ne^{7+}.

Contribution functions of Ne VIII and Mg VIII overlap considerably in temperature range just below 1 MK.
Contribution functions of Ne VIII and Mg IX are more similar at higher temperatures than that of Ne VIII and Mg VIII.

And yet, the same signature is visible which indicates that a temperature effect hardly plays a role.

In particular, Ne VIII /Na IX ratio shows that abundance anomaly is real and not a temperature effect.

Estimated FIP bias for Ne and Mg is 1.5 to 2.

What about stars?

Previous results (cf., Drake 2002):

Metal abundance in active stars → depleted.

Inactive stars → either a solar-like FIP effect or no FIP bias.

During flares → metal abundance increases, especially low-FIP elements.

A Glimpse of results obtained with XMM-Newton & Chandra:

Peculiar abundances: transition from a solar-like FIP to an inverse FIP effect with increasing activity.

(But it could be more complicated, e.g., Procyon, abundance increase at very low FIP, rare photospheric data).

The "inverse" FIP effect?

Inverse FIP effect, in which high-FIP elements are overabundant with respect to low-FIP elements, especially Ne seen in HR 1099 with XMM-Newton and Chandra (Drake *et al.* 2001).

From FIP to IFIP effect

i. Cool, inactive stars: solar-like FIP effect

ii. Hot, active stars: inverse FIP effect

iii. No FIP bias for stars with intermediate activity

More complicated?

In some active stars → abundances increase with increasing FIP, except at very low FIP where coronal abundances increase again.

The cool, inactive Procyon should display a strong solar-like FIP effect (Raassen *et al.* 2003).

However, it shows no FIP bias, consistently with previous EUVE results (Drake *et al.* 1995).

The "inverse" FIP effect?

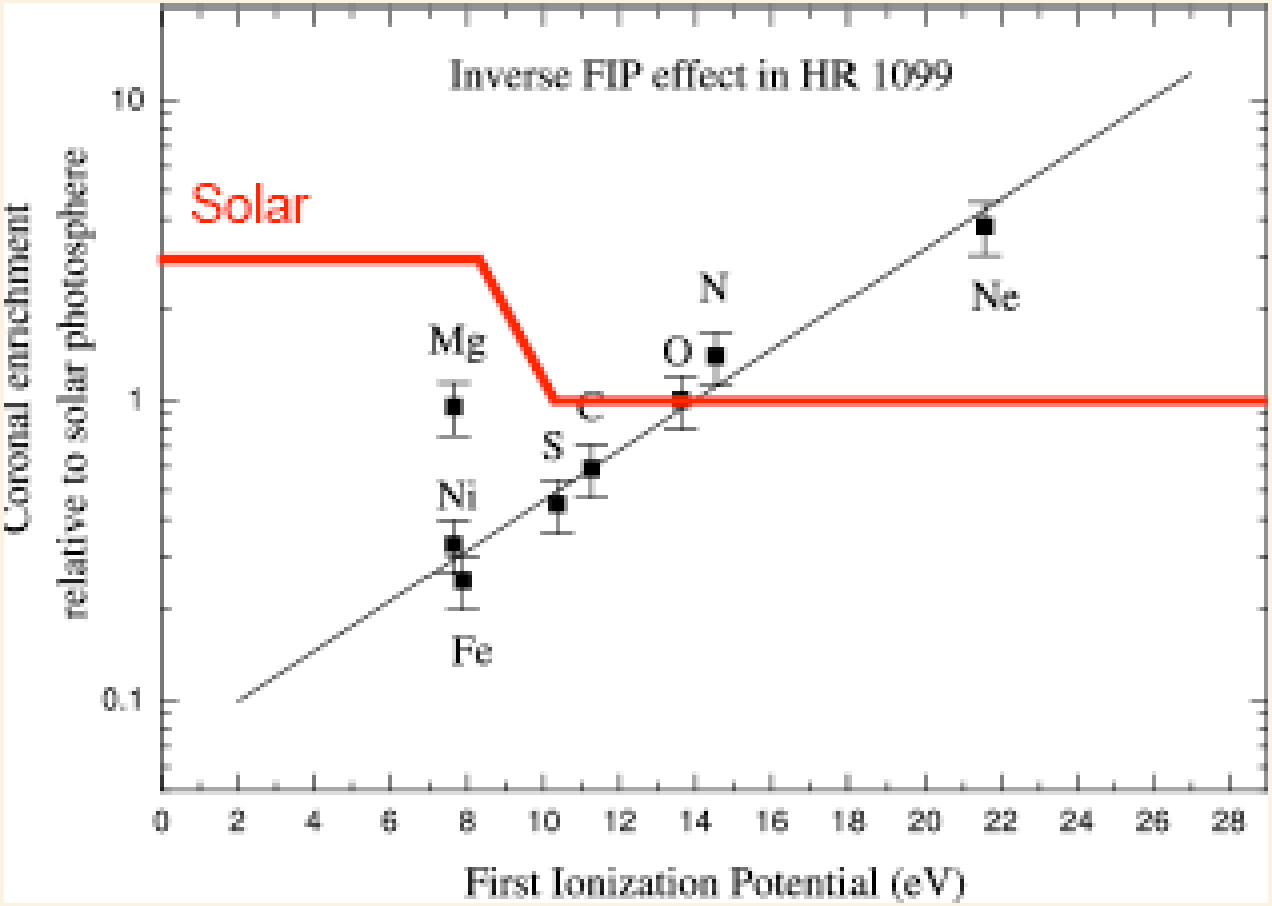

Inverse **FIP effect**, in which high-**FIP** elements are overabundant with respect to low-**FIP** elements, especially Ne seen in HR 1099 with XMM-Newton and Chandra. Brinkman *et al.* (2001); Drake *et al.* (2001)

A scenario for the FIP/IFIP effects?

Theoretical studies of the solar FIP effect already exist. We need a unified scenario that describes the transition from a solar-like FIP effect to an IFIP effect with increasing level of stellar magnetic activity.

Laming (2004) proposes such a unified picture by exploring the effects on the chromospheric plasma of the ponderomotive forces for Alfvén waves.

Abundance variations in flares

The picture is not unique:

i. **Abundances of low-FIP elements only increase** (Audard *et al.* 2001).

ii. **Abundances of all elements increase** (Osten *et al.* 2003, Güdel *et al.* 2004).

iii. **There is no abundance increase** (Huenemoerder *et al.* 2001)

Peculiar abundances:

Transition from a solar-like FIP to an inverse FIP effect with increasing activity.

(But it could be more complicated, e.g., Procyon, abundance increase at very low FIP, rare photospheric data).

Thank you